Research Article

The Modeling Method for Vibration Characteristics Analysis of Composite-Laminated Rotationally Stiffened Plate

Hong Zhang [1,2,3] **Yiqun Ding** [2] **Lin He,** [1,3] **Changgeng Shuai,** [1,3] **and Chao Jiang** [1,3]

[1]*Institute of Noise & Vibration, Naval University of Engineering, Wuhan 430033, China*
[2]*College of Mechanical and Electrical Engineering, Nanjing University of Aeronautics and Astronautics, Nanjing 210016, China*
[3]*National Key Laboratory on Ship Vibration & Noise, Wuhan 430033, China*

Correspondence should be addressed to Hong Zhang; zhanghongyuxin@outlook.com

The composite-laminated rotationally stiffened plate is widely applied in aviation, aerospace, ship, machinery, and other fields. For structural design and optimization, to investigate the vibration characteristics is important. In this paper, a modeling method of composite-laminated rotationally plate is established. The first-order shear deformation theory (FSDT) and the modified Fourier series are applied to construct the admissible displacement function of the stiffened plate-coupled systems. On this basis, the energy function of composite-laminated rotationally stiffened plate is established. Combined with the artificial virtual spring technology, the proposed theory could be used to analyze the vibration characteristics of composite-stiffened plate-coupled systems with various classical boundary conditions or arbitrary elastic boundary conditions. The Rayleigh–Ritz method is used to solve the energy function. Thus, the vibration characteristics of the composite-laminated rotationally stiffened plate are obtained and analyzed. The correctness of the theoretical analysis model was verified through modal experiments. On this basis, the effect of some important parameters on the vibration characteristics of stiffened plate structures is studied, such as the number, thickness, and width of the laminated stiffener, varying structural parameters, and different boundary conditions. This study can provide the theoretical basis for the vibration and noise reduction of such structures.

1. Introduction

The composite-laminated rotationally stiffened plate are basic structural element in aviation, aerospace, ship, machinery, and other fields, which makes it widely used in vehicle body, ship hull, and housing construction. Due to the special working environment, the plate structure is often subjected to complex dynamic loads, which causes mechanical vibration. In consequence, the vibration of composite-laminated rotationally stiffened plate is inevitably generated in engineering practice. To reveal the vibration characteristics and reduce vibration and noise, it is necessary to intensively investigate the vibration characteristics of composite-laminated rotationally stiffened plate. In recent years, rotary composite plate structures have been widely used in fields such as aerospace, shipbuilding, and ocean and have become an important direction for lightweight development. However, due to factors

such as impurities in the environment and the imperfectness of the process during the preparation process of composite materials, defects such as pores, impurities, and fiber curls will inevitably occur, which will affect the strength and stiffness of the structure. Therefore, reinforcing stiffeners are installed at appropriate positions of the plate structure through mechanical connections or adhesive bonding to effectively improve the overall strength and rigidity of the structure. The addition of reinforcing stiffeners results in discontinuous changes in material, mass, and damping parameters at the coupling interface between the plate and the reinforcing stiffeners. This leads to complex changes in waveform conversion and energy loss of vibration waves at the coupling interface between the plate and the reinforcing stiffeners. Therefore, it is of great significance to conduct theoretical modeling and vibration characteristics research on the composite-laminated rotationally stiffened plate.

Toshihiro et al. [1] studied the free vibration of an annular plate with radial stiffeners arranged at equal angle intervals on two surfaces of the plate using the Ritz method. The spline function was used as the allowable function for plate deflection to calculate the natural frequency and mode of vibration of the plate, and the influence of stiffeners on them was analyzed. Jafari et al. [2] conducted free vibration analysis of annular plates with nonuniform eccentric stiffeners and nonuniform spacing distribution stiffeners. The stiffeners were treated as discrete elements using the Ritz method, and the effects of nonuniform eccentric distribution and nonuniform spacing distribution on natural frequencies were analyzed. Qin et al. [3] modeled circular stiffened plates as a composite structure composed of circular plates and stiffeners and proposed a meshless method for bending and free vibration analysis of circular stiffened plates based on the first-order shear deformation theory. Golmakani et al. [4, 5], based on the first-order shear deformation theory, adopted the nonlinear von Karman plate theory, combined it with the finite element method, and studied the elastic large deflection mechanical behaviour of axisymmetric composite-stiffened circular and annular-laminated plates under transverse uniform load. The reinforcing stiffener is an orthotropic material with a circular shape. The effects of plate thickness, stiffener depth, thickness, and boundary conditions such as fixed support and simply supported on the nonlinear bending performance of reinforced circular and annular laminated plates were given. Ou et al. [6] used the weak form quadrature element method to analyze the nonlinear dynamic response of cylindrical composite stiffened laminated plates with dome shapes. The Newmark numerical integration method and the Newton Raphson iterative method are used to solve the nonlinear control equations. Examples including isotropic- and composite-laminated plates were provided to verify the effectiveness and accuracy of the formulas. The effects of geometric parameters, ply order, fixed, and simply supported boundary conditions on structural vibration were studied.

Peng et al. [7] proposed the meshless Galerkin method for geometrically nonlinear analysis of arbitrary polygon and circular stiffened plates based on the first-order shear deformation theory. Due to the absence of a grid in the model, reinforcing stiffeners can be placed anywhere on the slab, and changing the position of the reinforcing stiffeners does not require remeshing of the slab. This method explores the deflection calculation results of polygonal and circular stiffened plates under different boundary conditions, load forms, and reinforcement arrangement forms and proves the effectiveness of the calculation method through comparison with finite element software. Bhimaraddi et al. [8], based on the classical plate theory, used the method of combining the annular sector plate element and the curved beam element to carry out the finite element analysis of the orthogonal stiffened annular sector plate and verified the effectiveness of this method. Nagesh et al. [9] provided a detailed description of the noncoupled damage model based on the numerical model and used finite element analysis to evaluate the large deformation and ductile fracture failure of laterally stiffened circular plates with fixed boundary conditions under uniform pulse loads. Calin Itu et al. [10] proposed a method to improve the stiffness

of composite circular plates by installing radial stiffeners and studied the influence of different materials, thicknesses, and arrangement of stiffeners on the stiffness of composite circular plates under general boundary conditions using the finite element method. Turvey et al. [11] studied the elastic-plastic large deflection response of a single radial stiffened circular plate by establishing an Ilyushin full-section yield model for plates and an improved Von Mises yield model for stiffeners, combined with the finite difference mesh method. The effects of the depth of stiffener, boundary conditions for simple and fixed supports, and thickness of the plate on the elastic-plastic large deflection parameters are given.

In summary, although domestic and international scholars have conducted extensive research on the vibration characteristics of rotationally stiffened plate and shell structures, there are relatively a few research objects focused on composite materials, especially if the reinforcing stiffeners are also made of composite materials. We will only discuss a specific metal plate structural form, and when it comes to other structural forms, we will also need to carry out tedious modeling work. Moreover, the boundary conditions are relatively single, and there is relatively little research on complex elastic boundaries. Therefore, establishing a unified analysis model for the vibration characteristics of composite-stiffened plate and shell structures with complex boundaries is of great significance.

In this article, a unified analysis model for the vibration characteristics of the composite-laminated rotationally stiffened plate structure is established through the first-order shear deformation theory (FSDT) and the modified Fourier series method [12–14]; specifically, we establish a unified analysis model of composite-laminated rotationally stiffened plate structure under elastic boundary conditions. The structure is coupled with stiffened plate and stiffened beam. Combined with the modified Fourier series method and Rayleigh–Ritz method, the vibration characteristic of the model can be solved. After comparison and verification with the finite element method and experiment, the effect of some important parameters on the vibration characteristics of composite-laminated rotationally stiffened plate structure is studied, such as the number, thickness, and width of the stiffener, varying material parameters, and different boundary conditions.

2. Establishment of a Unified Analysis Model of Composite-Laminated Rotationally Stiffened Plate Structure

2.1. Model Description. The vibration analysis model of the composite-laminated rotationally stiffened plate is composed of the composite-laminated rotationally stiffened plate coupled with n laminated curved beams. The rotary plate structure includes annular sector plate, circular sector plate, annular plate, and circular plate. The specific model description is shown in Figure 1. The coordinates of the laminated plate are located in the coordinate system (o- z, θ, r) as shown in the figure. The coordinates of the nth laminated curved beam are located in the coordinate system ($o_n - z_n$, θ_n, x_n) as shown in the figure. The inner radius and outer radius of the composite-laminated rotationally

stiffened plate in the stiffened plates are R_1 and R_2, where $R_p = R_2 - R_1$ and the thickness is h_p. The curvature radius of the laminated curved beam is R_{bn}, width is b_n, and thickness is h_n. The rotation angle of the entire stiffened plate is ϑ. According to the different values of geometric parameters, there are the following models:(1) when $0 < R_1 < R_2$, $\vartheta = 360°$, the structure is an annular stiffened composite plate; (2) when $0 < R_1 < R_2$, $0 < \vartheta < 360°$, the structure is an annular fan-shaped stiffened composite plate; (3) when $R_1 = 0$, $\vartheta = 360°$, the structure is a circular stiffened composite plate; and (4) when $R_1 = 0, 0 < \vartheta < 360°$, the structure is fan-shaped stiffened composite plate.

As shown in Figure 2(a), at the edge of the composite-laminated rotationally stiffened plate, general boundary conditions are defined by introducing three groups of linear springs k_u, k_v, k_w and two groups of torsion springs K_r, K_θ along the u, v, w directions, respectively [15–17], continuous distribution of spring groups along the boundary. $k_{\theta0}^u, k_{\theta0}^v, k_{\theta0}^w$, $K_{\theta0}^r$, and $K_{\theta0}^\theta$ represent five sets of boundary springs at the boundary $\theta = 0°$. The same can be said for the boundary of the $\theta = \vartheta$, $r = 0$, and $r = R_p$ spring and can be represented by this method. For sector-stiffened composite plates, the stiffness of the boundary spring at the boundary $r = 0$ is set to 0; for annular stiffened composite plates, the stiffness of the boundary spring at the boundary $\theta = 0°$ and $\theta = 360°$ is set to 0; and for circular stiffened composite plate, the stiffness of the boundary spring at the boundary $r = 0, \theta = 0°$ and $\theta = 360°$ is set to 0. When rotating angle $\vartheta = 360°$, laminated plates (the nth laminated beam) in the composite-laminated rotationally stiffened plate will produce the coupling boundary as shown in Figure 2(b) (Figure 2(c)) at the two edges of $\theta = 0°$ and $\theta = 360°$. Three sets of linear coupled springs $k_{uc}^p, k_{vc}^p, k_{wc}^p$ ($k_{uc}^{b_n}$, $k_{vc}^{b_n}$, and $k_{wc}^{b_n}$) and two sets of torsional springs $K_{rc}^p, K_{\theta c}^p$ ($K_{xc}^{b_n}$, and $K_{\theta c}^{b_n}$) are uniformly arranged on the coupling boundary to realize the coupling of the composite-laminated rotationally stiffened plate. Figure 2(d) shows the uniformly arranged coupling springs between the laminated plate and laminated curved beam in composite-laminated rotationally stiffened plate, including three sets of linear coupling springs, i.e., k_{uc}^{cp}, k_{vc}^{cp}, and k_{wc}^{cp} and two sets of torsional springs, i.e., K_{xc}^{cp} and K_{yc}^{cp}.

2.2. Construction of Admissible Displacement Functions.
According to the first-order shear deformation theory (FSDT), the displacement components U_p, V_p, W_p and U_{bn}, V_{bn}, W_{bn} at any point on the laminated plate and laminated curved beam of the composite-laminated rotationally stiffened plate structure can be expressed as follows:

$$\begin{cases} U_p(r, \theta, z, t) = u_p(r, \theta, t) + z\phi_{rp}(r, \theta, t), \\ V_p(r, \theta, z, t) = v_p(r, \theta, t) + z\phi_{\theta p}(r, \theta, t), \\ W_p(r, \theta, z, t) = w_p(r, \theta, t). \end{cases} \quad (1)$$

$$\begin{cases} U_{bn}(\theta_n, z, t) = u_{bn}(\theta_n, t) + z\phi_{xbn}(\theta_n, t), \\ V_{bn}(\theta_n, z, t) = v_{bn}(\theta_n, t) + z\phi_{\theta bn}(\theta_n, t), \\ W_{bn}(\theta_n, z, t) = w_{bn}(\theta_n, t). \end{cases} \quad (2)$$

where u_p, v_p, and w_p represent the displacement of the middle plane in the r, θ, and z directions of the composite-laminated rotationally stiffened plate, ϕ_{rp} and $\phi_{\theta p}$ indicate its lateral rotation in θ and r direction; u_{bn}, v_{bn}, and w_{bn} indicate the displacement of the middle plane of the nth laminated curved beam in x_n, θ_n and z_n directions, and ϕ_{xbn} and $\phi_{\theta bn}$ indicate its lateral rotation in θ_n and x_n direction. t represents a time variable.

Based on the improved Fourier series method, the admissible displacement functions of laminated plates in composite-laminated rotationally stiffened plates are established. The admissible displacement functions established in this method can ignore the influence of the boundary conditions, and the auxiliary polynomial is introduced to eliminate the discontinuity and jump phenomenon of the displacement function at the boundary. The specific expression is

$$u_p(r, \theta, t) = e^{-j\omega t}\left(\mathbf{\Phi}_u^M(r, \theta) + \sum_{N_q=1}^{2} \mathbf{\Phi}_u^{N_q}(r, \theta)\right)\mathbf{A}_{mn},$$

$$v_p(r, \theta, t) = e^{-j\omega t}\left(\mathbf{\Phi}_v^M(r, \theta) + \sum_{N_q=1}^{2} \mathbf{\Phi}_v^{N_q}(r, \theta)\right)\mathbf{B}_{mn},$$

$$w_p(r, \theta, t) = e^{-j\omega t}\left(\mathbf{\Phi}_w^M(r, \theta) + \sum_{N_q=1}^{2} \mathbf{\Phi}_w^{N_q}(r, \theta)\right)\mathbf{C}_{mn}, \quad (3)$$

$$\phi_{rp}(r, \theta, t) = e^{-j\omega t}\left(\mathbf{\Phi}_{\phi_r}^M(r, \theta) + \sum_{N_q=1}^{2} \mathbf{\Phi}_{\phi_r}^{N_q}(r, \theta)\right)\mathbf{D}_{mn},$$

$$\phi_{\theta p}(r, \theta, t) = e^{-j\omega t}\left(\mathbf{\Phi}_{\phi_\theta}^M(r, \theta) + \sum_{N_q=1}^{2} \mathbf{\Phi}_{\phi_\theta}^{N_q}(r, \theta)\right)\mathbf{E}_{mn}.$$

By using the same theoretical method, the admissible displacement functions of the laminated curved beam in composite-laminated rotationally stiffened plate can also be established as follows:

$$u_{bn}(\theta_n, t) = e^{-j\omega t}\left(\mathbf{\Psi}_{u_n}^\Omega(\theta_n) + \sum_{\Theta_q=1}^{2} \mathbf{\Psi}_{u_n}^{\Theta_q}(\theta_n)\right)\mathbf{A}_l$$

$$v_{bn}(\theta_n, t) = e^{-j\omega t}\left(\mathbf{\Psi}_{v_n}^\Omega(\theta_n) + \sum_{\Theta_q=1}^{2} \mathbf{\Psi}_{v_n}^{\Theta_q}(\theta_n)\right)\mathbf{B}_l$$

$$w_{bn}(\theta_n, t) = e^{-j\omega t}\left(\mathbf{\Psi}_{w_n}^\Omega(\theta_n) + \sum_{\Theta_q=1}^{2} \mathbf{\Psi}_{w_n}^{\Theta_q}(\theta_n)\right)\mathbf{C}_l \quad (4)$$

$$\phi_{xbn}(\theta_n, t) = e^{-j\omega t}\left(\mathbf{\Psi}_{\phi_{rn}}^\Omega(\theta_n) + \sum_{\Theta_q=1}^{2} \mathbf{\Psi}_{\phi_{rn}}^{\Theta_q}(\theta_n)\right)\mathbf{D}_l$$

$$\phi_{\theta bn}(\theta_n, t) = e^{-j\omega t}\left(\mathbf{\Psi}_{\phi_{\theta n}}^\Omega(\theta_n) + \sum_{\Theta_q=1}^{2} \mathbf{\Psi}_{\phi_{\theta n}}^{\Theta_q}(\theta_n)\right)\mathbf{E}_l.$$

The displacement supplement polynomial of composite-laminated plate can be expressed as $\mathbf{\Phi}^M$ and $\mathbf{\Phi}^{Nq}$ ($N_q = 1, 2$). The displacement supplement polynomial of the
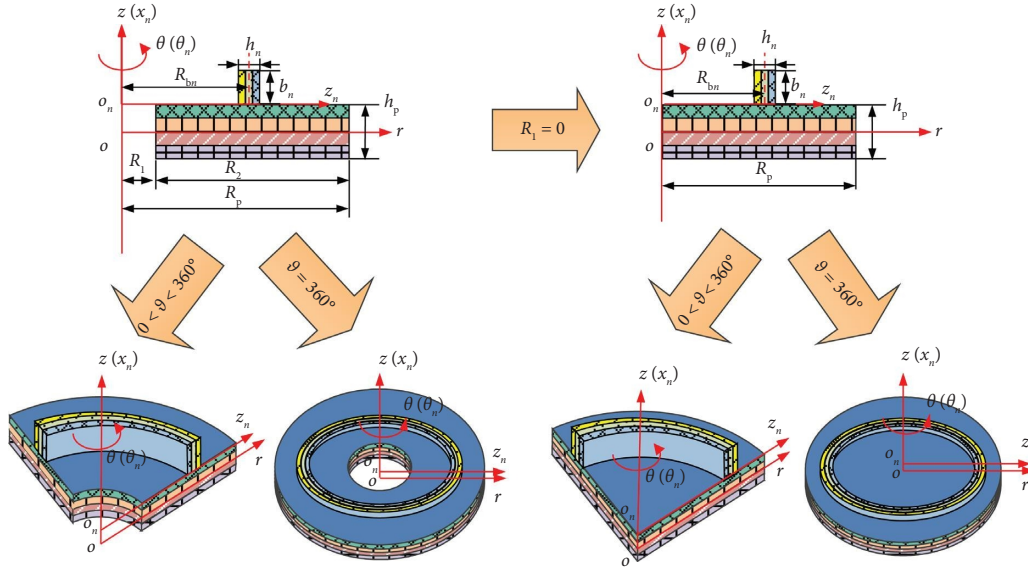
Figure 1: Unified model of composite ring fan-shaped, annular, fan-shaped, and circular stiffened plates.

(a)

(b)

(c)

(d)
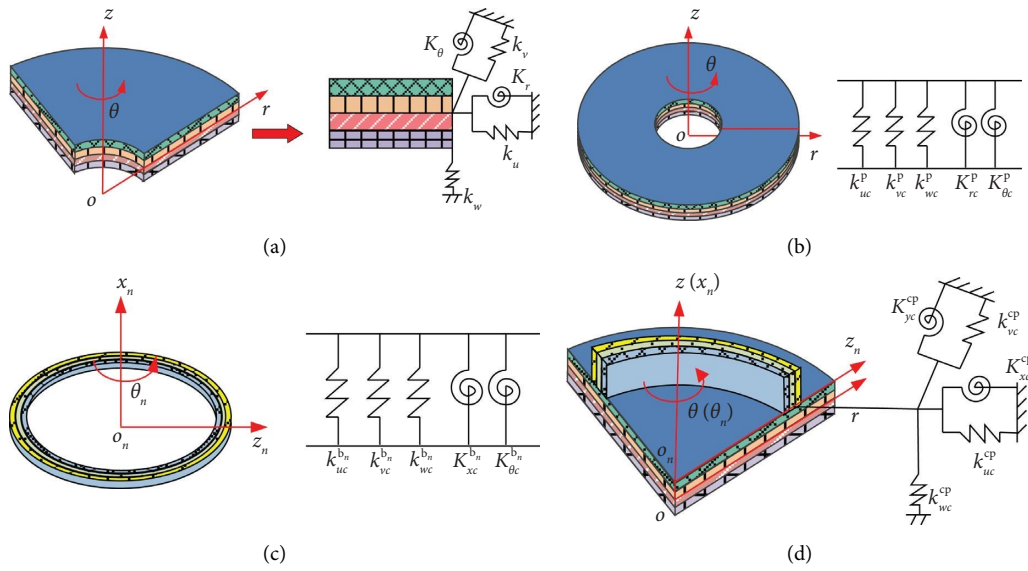
Figure 2: Boundary spring and coupling spring of composite-laminated rotationally stiffened plate. (a) Laminated plate boundary spring. (b) Laminated plate coupling spring. (c) Laminated curved beam coupling spring. (d) Coupling springs of plates and beams.

nth laminated curved beam can be expressed as Ψ_n^{Ω} and $\Psi_n^{\Theta q}$ ($\Theta_q = 1, 2$). Professor Li [18, 19] proposed the modified Fourier series method, which expressed the displacement function of beam or plate structure in the form of traditional Fourier series plus the auxiliary function. It must be noted here that the main function of the auxiliary function is to enable the traditional Fourier series and the corresponding derivatives to avoid the occurrence of nonexistent or jumping phenomena at the boundary position. At present, the commonly used auxiliary function forms are Legendre polynomial, series polynomial, and complete series. The auxiliary function used in this paper is the complete series method. Where $\mathbf{A}_{mn}, \mathbf{B}_{mn}, \mathbf{C}_{mn}, \mathbf{D}_{mn}$ and $\mathbf{E}_{mn}$ represent the unknown two-dimensional Fourier coefficient vectors of the admissible displacement functions of the laminated plate, these parameters can be expressed as follows:

$$\boldsymbol{\Phi}_u^M = \boldsymbol{\Phi}_w^M = \boldsymbol{\Phi}_v^M = \boldsymbol{\Phi}_{\phi_r}^M = \boldsymbol{\Phi}_{\phi_\theta}^M = \left\{ \begin{array}{l} \cos \lambda_0^\alpha r \cos \lambda_0^\beta \theta, \cdots, \cos \lambda_m^\alpha r \cos \lambda_n^\beta \theta, \cdots, \\ \cos \lambda_0^\alpha r \cos \lambda_N^b \theta, \cdots \cos \lambda_M^\alpha r \cos \lambda_N^\beta \theta, \end{array} \right\},$$

$$\boldsymbol{\Phi}_u^{N_1} = \boldsymbol{\Phi}_v^{N_1} = \boldsymbol{\Phi}_w^{N_1} = \boldsymbol{\Phi}_{\phi_r}^{N_1} = \boldsymbol{\Phi}_{\phi_\theta}^{N_1} = \left\{ \begin{array}{l} \sin\left(\lambda_{-2}^\alpha r\right)\cos\left(\lambda_0^\beta \theta\right), \cdots, \sin\left(\lambda_{-2}^\alpha r\right)\cos\left(\lambda_n^\beta \theta\right), \cdots, \\ \sin\left(\lambda_{-2}^\alpha r\right)\cos\left(\lambda_N^\beta \theta\right), \cdots, \sin\left(\lambda_{-1}^\alpha r\right)\cos\left(\lambda_N^\beta \theta\right). \end{array} \right\}, \tag{5}$$

$$\boldsymbol{\Phi}_u^{N_2} = \boldsymbol{\Phi}_v^{N_2} = \boldsymbol{\Phi}_w^{N_2} = \boldsymbol{\Phi}_{\phi_r}^{N_2} = \boldsymbol{\Phi}_{\phi_\theta}^{N_2} = \left\{ \begin{array}{l} \cos\left(\lambda_0^\alpha r\right)\sin\left(\lambda_{-2}^\beta \theta\right), \cos\left(\lambda_0^\alpha r\right)\sin\left(\lambda_{-1}^\beta \theta\right), \cdots, \\ \cos\left(\lambda_m^\alpha r\right)\sin\left(\lambda_{-2}^\beta \theta\right), \cdots, \cos\left(\lambda_M^\alpha r\right)\sin\left(\lambda_{-1}^\beta \theta\right). \end{array} \right\},$$

$$\mathbf{A}_{mn} = \left\{ \begin{array}{l} A_{0,0}^1, \cdots, A_{0,n}^1, \cdots, A_{m,n}^1, \cdots, A_{M,N}^1, A_{-2,0}^2, \cdots, A_{-2,n}^2, \cdots, \\ A_{-2,N}^2, \cdots, A_{-1,N}^2, A_{0,-2}^3, A_{0,-1}^3, \cdots, A_{m,-2}^3, \cdots, A_{M,-1}^3 \end{array} \right\}^T,$$

$$\mathbf{B}_{mn} = \left\{ \begin{array}{l} B_{0,0}^1, \cdots, B_{0,n}^1, \cdots, B_{m,n}^1, \cdots, B_{M,N}^1, B_{-2,0}^2, \cdots, B_{-2,n}^2, \cdots, \\ B_{-2,N}^2, \cdots, B_{-1,N}^2, B_{0,-2}^3, B_{0,-1}^3, \cdots, B_{m,-2}^3, \cdots, B_{M,-1}^3. \end{array} \right\}^T,$$

$$\mathbf{C}_{mn} = \left\{ \begin{array}{l} C_{0,0}^1, \cdots, C_{0,n}^1, \cdots, C_{m,n}^1, \cdots, C_{M,N}^1, C_{-2,0}^2, \cdots, C_{-2,n}^2, \cdots, \\ C_{-2,N}^2, \cdots, C_{-1,N}^2, C_{0,-2}^3, C_{0,-1}^3, \cdots, C_{m,-2}^3, \cdots, C_{M,-1}^3. \end{array} \right\}^T, \tag{6}$$

$$\mathbf{D}_{mn} = \left\{ \begin{array}{l} D_{0,0}^1, \cdots, D_{0,n}^1, \cdots, D_{m,n}^1, \cdots, D_{M,N}^1, D_{-2,0}^2, \cdots, D_{-2,n}^2, \cdots, \\ D_{-2,N}^2, \cdots, D_{-1,N}^2, D_{0,-2}^3, D_{0,-1}^3, \cdots, D_{m,-2}^3, \cdots, D_{M,-1}^3. \end{array} \right\}^T,$$

$$\mathbf{E}_{mn} = \left\{ \begin{array}{l} E_{0,0}^1, \cdots, E_{0,n}^1, \cdots, E_{m,n}^1, \cdots, E_{M,N}^1, E_{-2,0}^2, \cdots, E_{-2,n}^2, \cdots, \\ E_{-2,N}^2, \cdots, E_{-1,N}^2, E_{0,-2}^3, E_{0,-1}^3, \cdots, E_{m,-2}^3, \cdots, E_{M,-1}^3. \end{array} \right\}^T,$$

where $\mathbf{A}_l, \mathbf{B}_l, \mathbf{C}_l, \mathbf{D}_l,$ and $\mathbf{E}_l$ represent the unknown one-dimensional Fourier coefficient vector of the admissible displacement functions of the laminated curved beam, which can be expressed as follows:

$$\boldsymbol{\Psi}_{u_n}^\Omega = \boldsymbol{\Psi}_{v_n}^\Omega = \boldsymbol{\Psi}_{w_n}^\Omega = \boldsymbol{\Psi}_{\phi_{xn}}^\Omega = \boldsymbol{\Psi}_{\phi_{\theta n}}^\Omega = \left\{ \cos \lambda_0^{\alpha_n} \theta_n, \cdots, \cos \lambda_l^{\alpha_n} \theta_n, \cdots \cos \lambda_L^{\alpha_n} \theta_n \right\},$$

$$\boldsymbol{\Psi}_{u_n}^{\Theta_1} = \boldsymbol{\Psi}_{v_n}^{\Theta_1} = \boldsymbol{\Psi}_{w_n}^{\Theta_1} = \boldsymbol{\Psi}_{\phi_{xn}}^{\Theta_1} = \boldsymbol{\Psi}_{\phi_{\theta n}}^{\Theta_1} = \frac{\alpha_n}{2\pi} \sin\left(\frac{\pi \theta_n}{2\alpha_n}\right) + \frac{\alpha_n}{2\pi} \sin\left(\frac{3\pi \theta_n}{2\alpha_n}\right), \tag{7}$$

$$\boldsymbol{\Psi}_{u_n}^{\Theta_2} = \boldsymbol{\Psi}_{v_n}^{\Theta_2} = \boldsymbol{\Psi}_{w_n}^{\Theta_2} = \boldsymbol{\Psi}_{\phi_{xn}}^{\Theta_2} = \boldsymbol{\Psi}_{\phi_{\theta n}}^{\Theta_2} = -\frac{\alpha_n}{2\pi} \cos\left(\frac{\pi \theta_n}{2\alpha_n}\right) + \frac{\alpha_n}{2\pi} \cos\left(\frac{3\pi \theta_n}{2\alpha_n}\right),$$

$$\mathbf{A}_l = \left\{ A_0, A_1, \cdots, A_l, \cdots, A_L, a_1, a_2 \right\}^T,$$

$$\mathbf{B}_l = \left\{ B_0, B_1, \cdots, B_l, \cdots, A_L, b_1, b_2 \right\}^T,$$

$$\mathbf{C}_l = \left\{ C_0, C_1, \cdots, C_l, \cdots, C_L, c_1, c_2 \right\}^T, \tag{8}$$

$$\mathbf{D}_l = \left\{ D_0, D_1, \cdots, D_l, \cdots, D_L, d_1, d_2 \right\}^T,$$

$$\mathbf{E}_l = \left\{ E_0, E_1, \cdots, E_l, \cdots, E_L, e_1, e_2 \right\}^T,$$

where $\lambda_m^\alpha = m\pi/\alpha$, $\lambda_n^\beta = n\pi/\beta$, and $\lambda_l^{\alpha_n} = l\pi/\alpha_n$.

2.3. Stress-Strain and Displacement Relations. According to the relevant knowledge of elastic mechanics, the normal strain and shear strain at any point on the composite-laminated plate and laminated curved beams can be defined by strain and curvature change of the middle surface as follows:

$$
\left\{ \begin{array}{l} \varepsilon_r^P = \varepsilon_r^{p0} + z\chi_r^p, \\ \varepsilon_\theta^P = \varepsilon_\theta^{p0} + z\chi_\theta^p, \end{array} \right. \left\{ \begin{array}{l} \gamma_{r\theta}^P = \gamma_{r\theta}^{p0} + z\chi_{r\theta}^p, \\ \gamma_{rz}^P = \gamma_{rz}^{p0}, \\ \gamma_{\theta z}^P = \gamma_{\theta z}^{p0}, \end{array} \right. \tag{9}
$$

$$
\varepsilon_\theta^{bn} = \varepsilon_\theta^{bn0} + z\chi_\theta^{bn} \left\{ \begin{array}{l} \gamma_{\theta x}^{bn} = \gamma_{\theta x}^{bn0} + z\chi_{\theta x}^{bn}, \\ \gamma_{\theta z}^{bn} = \gamma_{\theta z}^{bn0}, \\ \gamma_{xz}^{bn} = \gamma_{xz}^{bn0}, \end{array} \right. \tag{10}
$$

in which ε_r^{p0}, ε_θ^{p0}, $\gamma_{r\theta}^{p0}$, γ_{rz}^{p0}, and $\gamma_{\theta z}^{p0}$ represent the strain component on the middle plane of laminated plates, χ_r^p, χ_θ^p, and $\chi_{r\theta}^p$ represent the component of curvature change on the middle plane of laminated plates, ε_θ^{bn0}, $\gamma_{\theta x}^{bn0}$, $\gamma_{\theta z}^{bn0}$, and γ_{xz}^{bn0} represent the strain component on the middle plane of the nth laminated curved beam, and χ_θ^{bn} and $\chi_{\theta x}^{bn}$ represent the component of curvature change on the middle plane of a laminated curved beam. The specific expression is

$$
\varepsilon_r^{p0} = \frac{\partial u_p}{\partial r},
$$

$$
\varepsilon_\theta^{p0} = \frac{\partial v_p}{r\partial\theta} + \frac{u_p}{r},
$$

$$
\gamma_{r\theta}^{p0} = \frac{\partial v_p}{\partial r} + \frac{\partial u_p}{r\partial\theta} - \frac{v_p}{r},
$$

$$
\gamma_{rz}^{p0} = \frac{\partial w_p}{\partial r} + \phi_{rp},
$$

$$
\gamma_{\theta z}^{p0} = \phi_{\theta p},
$$

$$
\chi_r^p = \frac{\partial \phi_{rp}}{\partial r},
$$

$$
\chi_\theta^p = \frac{\partial \phi_{\theta p}}{r\partial\theta} + \frac{\phi_{rp}}{r},
$$

$$
\chi_{r\theta}^p = \frac{\partial \phi_{\theta p}}{\partial r} + \frac{\partial \phi_{rp}}{r\partial\theta} - \frac{\phi_{\theta p}}{r},
$$

$$
\varepsilon_\theta^{bn0} = \frac{\partial v_{bn}}{R_n\partial\theta_n} + \frac{w_{bn}}{R_n},
$$

$$
\gamma_{\theta x}^{bn0} = \frac{\partial u_{bn}}{R_n\partial\theta_n},
$$

$$
\gamma_{\theta z}^{p0} = \frac{\partial w_{bn}}{R_n\partial\theta_n} - \frac{v_{bn}}{R_n} + \phi_{\theta bn},
$$

$$
\gamma_{xz}^{bn0} = \phi_{xbn},
$$

$$
\chi_\theta^{bn} = \frac{\partial \phi_{\theta bn}}{R_n\partial\theta_n},
$$

$$
\chi_{\theta x}^{bn} = \frac{\partial \phi_{xbn}}{R_n\partial\theta_n}. \tag{12}
$$

According to Hooke's law, the corresponding stress-strain relationship of laminated plate and laminated curved beam at the k-th layer can be obtained as follows:

$$
\left\{ \begin{array}{c} \sigma_r^p \\ \sigma_\theta^p \\ \tau_{r\theta}^p \\ \tau_{rz}^p \\ \tau_{\theta z}^p \end{array} \right\} = \begin{bmatrix} \overline{Q_{11}^k} & \overline{Q_{12}^k} & 0 & 0 & \overline{Q_{16}^k}, \\ \overline{Q_{21}^k} & \overline{Q_{22}^k} & 0 & 0 & \overline{Q_{26}^k}, \\ 0 & 0 & \overline{Q_{44}^k} & \overline{Q_{45}^k} & 0 \\ 0 & 0 & \overline{Q_{54}^k} & \overline{Q_{55}^k} & 0 \\ \overline{Q_{61}^k} & \overline{Q_{62}^k} & 0 & 0 & \overline{Q_{66}^k}. \end{bmatrix} \left\{ \begin{array}{c} \varepsilon_r^p \\ \varepsilon_\theta^p \\ \gamma_{r\theta}^p \\ \gamma_{rz}^p \\ \gamma_{\theta z}^p \end{array} \right\}, \tag{13}
$$

$$
\left\{ \begin{array}{c} \sigma_\theta^{bn} \\ \tau_{\theta x}^{bn} \\ \tau_{\theta z}^{bn} \\ \tau_{xz}^{bn} \end{array} \right\} = \begin{bmatrix} \overline{Q_{22}^k} & 0 & 0 & \overline{Q_{26}^k}, \\ 0 & \overline{Q_{44}^k} & \overline{Q_{45}^k} & 0 \\ 0 & \overline{Q_{54}^k} & \overline{Q_{55}^k} & 0 \\ \overline{Q_{62}^k} & 0 & 0 & \overline{Q_{66}^k}. \end{bmatrix} \left\{ \begin{array}{c} \varepsilon_\theta^{bn} \\ \gamma_{\theta x}^{bn} \\ \gamma_{\theta z}^{bn} \\ \gamma_{xz}^{bn} \end{array} \right\}, \tag{14}
$$

where $\overline{Q_{ij}^k}$ $(i, j = 1, 2, \ldots, 6)$ is the relevant stiffness coefficient, which can be obtained from the following equation:

$$
\begin{bmatrix} \overline{Q_{11}^k} & \overline{Q_{12}^k} & 0 & 0 & \overline{Q_{16}^k}, \\ \overline{Q_{21}^k} & \overline{Q_{22}^k} & 0 & 0 & \overline{Q_{26}^k}, \\ 0 & 0 & \overline{Q_{44}^k} & \overline{Q_{45}^k} & 0 \\ 0 & 0 & \overline{Q_{54}^k} & \overline{Q_{55}^k} & 0 \\ \overline{Q_{61}^k} & \overline{Q_{62}^k} & 0 & 0 & \overline{Q_{66}^k}. \end{bmatrix} = \mathbf{T} \begin{bmatrix} Q_{11}^k & Q_{12}^k & 0 & 0 & 0 \\ Q_{21}^k & Q_{22}^k & 0 & 0 & 0 \\ 0 & 0 & Q_{44}^k & 0 & 0 \\ 0 & 0 & 0 & Q_{55}^k & 0 \\ 0 & 0 & 0 & 0 & Q_{66}^k \end{bmatrix} \mathbf{T}^T. \tag{15}
$$

In (15), $\mathbf{T}$ is the transformation matrix, which is defined as follows, where θ_k is the included angle between the main direction and the r direction (the laminated curved beam is the x_n direction), that is, the angle-ply.

$$
\mathbf{T} = \begin{bmatrix} \cos^2\theta_k & \sin^2\theta_k & 0 & 0 & -2\sin\theta_k\cos\theta_k, \\ \sin^2\theta_k & \cos^2\theta_k & 0 & 0 & 2\sin\theta_k\cos\theta_k \\ 0 & 0 & \cos\theta_k & \sin\theta_k & 0 \\ 0 & 0 & -\sin\theta_k & \cos\theta_k & 0 \\ \sin\theta_k\cos\theta_k & -\sin\theta_k\cos\theta_k & 0 & 0 & \cos^2\theta_k - \sin^2\theta_k. \end{bmatrix}, \tag{16}
$$

in which Q_{ij}^k $(i, j = 1, 2, \ldots, 6)$ represents the material coefficient of the k layer of the laminated plate (laminated curved beam), which value can be obtained according to the engineering constant of the k layer of the laminated plate (laminated curved beam) as follows:

$$
Q_{11}^k = \frac{E_1}{1 - \mu_{12}\mu_{21}},
$$

$$
Q_{12}^k = \frac{\mu_{12}E_2}{1 - \mu_{12}\mu_{21}} = Q_{21}^k,
$$

$$
Q_{22}^k = \frac{E_2}{1 - \mu_{12}\mu_{21}}, \tag{17}
$$

$$
Q_{44}^k = G_{23},
$$

$$
Q_{55}^k = G_{13} \quad Q_{66}^k = G_{12},
$$

where E_1 and E_2 are Young's modulus; $G_{12}, G_{13},$ and G_{23} are shear modulus. The relationship between Poisson's ratio μ_{12} and μ_{21} is as follows: $\mu_{12}E_2 = \mu_{21}E_1$.

The forces and moments experienced by laminated plate and laminated curved beam are obtained by integrating the stresses on the plane. From one layer of laminated plate and laminated curved beam to the other layer, by integrating the thickness, we can obtain

$$
\begin{bmatrix} N_r^p \\ N_\theta^p \\ N_{r\theta}^p \\ M_r^p \\ M_\theta^p \\ M_{r\theta}^p \end{bmatrix} = \begin{bmatrix} A_{11} & A_{12} & A_{16} & B_{11} & B_{12} & B_{16} \\ A_{12} & A_{22} & A_{26} & B_{12} & B_{22} & B_{26} \\ A_{16} & A_{26} & A_{66} & B_{16} & B_{26} & B_{66} \\ B_{11} & B_{12} & B_{16} & D_{11} & D_{12} & D_{16} \\ B_{12} & B_{22} & B_{26} & D_{12} & D_{22} & D_{26} \\ B_{16} & B_{26} & B_{66} & D_{16} & D_{26} & D_{66} \end{bmatrix} \begin{bmatrix} \varepsilon_r^{p0} \\ \varepsilon_\theta^{p0} \\ \gamma_{r\theta}^{p0} \\ \chi_r^p \\ \chi_\theta^p \\ \chi_{r\theta}^p \end{bmatrix}, \tag{18}
$$

$$
\begin{bmatrix} Q_\theta^p \\ Q_r^p \end{bmatrix} = \overline{\kappa_s} \begin{bmatrix} A_{44} & A_{45} \\ A_{45} & A_{55} \end{bmatrix} \begin{bmatrix} \gamma_{\theta z}^{p0} \\ \gamma_{rz}^{p0} \end{bmatrix}, \tag{19}
$$

$$
\begin{bmatrix} N_\theta^{bn} \\ N_{\theta x}^{bn} \\ M_\theta^{bn} \\ M_{\theta x}^{bn} \end{bmatrix} = \begin{bmatrix} A_{22} & A_{26} & B_{22} & B_{26} \\ A_{26} & A_{66} & B_{26} & B_{66} \\ B_{22} & B_{26} & D_{22} & D_{26} \\ B_{26} & B_{66} & D_{26} & D_{66} \end{bmatrix} \begin{bmatrix} \varepsilon_\theta^{bn0} \\ \gamma_{\theta x}^{bn0} \\ \chi_\theta^{bn} \\ \chi_{\theta x}^{bn} \end{bmatrix}, \tag{20}
$$

$$
\begin{bmatrix} Q_x^{bn} \\ Q_\theta^{bn} \end{bmatrix} = \overline{\kappa_s} \begin{bmatrix} A_{44} & A_{45} \\ A_{45} & A_{55} \end{bmatrix} \begin{bmatrix} \gamma_{xz}^{bn0} \\ \gamma_{\theta z}^{bn0} \end{bmatrix}, \tag{21}
$$

$$
A_{ij} = \sum_{k=1}^{N_L} \overline{Q_{ij}^k} (Z_{k+1} - Z_k),
$$
$$
B_{ij} = \frac{1}{2} \sum_{k=1}^{N_L} \overline{Q_{ij}^k} (Z_{k+1}^2 - Z_k^2), \tag{22}
$$
$$
D_{ij} = \frac{1}{3} \sum_{k=1}^{N_L} \overline{Q_{ij}^k} (Z_{k+1}^3 - Z_k^3),
$$

in which N_r^p, N_θ^p, and $N_{r\theta}^p$ represent the resultant force in the plane of the laminated plate, M_r^p, M_θ^p, and $M_{r\theta}^p$ represent bending and torsional moments in the plane of the laminated plate, and Q_θ^p and Q_r^p are the resultant force of the horizontal shear force of the laminated plate. N_θ^{bn} and $N_{\theta x}^{bn}$ represent the resultant force in the plane of the laminated curved beam, M_θ^{bn} and $M_{\theta x}^{bn}$ represent the bending and torsional moments in the plane of the laminated curved beam, and Q_x^{bn} and Q_θ^{bn} are the resultant force of the horizontal shear force in the plane of the laminated curved beam. $\overline{\kappa_s}$ is the shear correction coefficient [20], and N_L represents the number of layers of laminated plates or laminated curved beams. Z_k is the thickness coordinate value of the bottom surface of the k

layer, and Z_{k+1} is the thickness coordinate value of the upper surface.

2.4. Energy Functions and the Solving Process. According to the principle of energy, the energy function of the rotational stiffened composite plate can be listed, and the unknown coefficient can be solved by the Rayleigh–Ritz method. The Lagrange equation of the stiffened plate can be expressed as follows:

$$
L_P = T_P - U_P - U_{P-\text{coupling}} - U_{SP} - W_{P\&B_n} + W_F, \tag{23}
$$

$$
L_{B_n} = T_{B_n} - U_{B_n} - U_{B_n-\text{coupling}} - W_{P\&B_n}, \tag{24}
$$

where T_P and T_{B_n} represent the total kinetic energy of the laminated plate and the nth laminated curved beam of the rotational stiffened plate, U_P and U_{B_n} are the total potential energy of the laminated plate and the nth laminated curved beam, $U_{P-\text{coupling}}$ and $U_{B_n-\text{coupling}}$ represent the coupled potential of laminated plate and nth laminated beam when $\vartheta = 360°$, U_{SP} represents the potential energy of boundary spring of the laminated plate, $W_{P\&B_n}$ is the coupled potential

generated when the laminated plate and the nth laminated curved beam are coupled, and W_F represents the work done by simple harmonic point force F on rotational stiffened composite plate.

The total kinetic energy of laminated composite plates T_P and the total kinetic energy of the nth laminated beam T_{B_n} can be written as follows:

$$T_P = \frac{1}{2} \int_0^{R_P} \int_0^{\vartheta} \left\{ \begin{array}{l} I_{p0}\left(\frac{\partial u_p}{\partial t}\right)^2 + 2I_{p1}\left(\frac{\partial u_p}{\partial t}\right)\left(\frac{\partial \phi_{rp}}{\partial t}\right) + I_{p2}\left(\frac{\partial \phi_{rp}}{\partial t}\right)^2 + I_{p0}\left(\frac{\partial v_p}{\partial t}\right)^2 \\ \\ + 2I_{p1}\left(\frac{\partial v_p}{\partial t}\right)\left(\frac{\partial \phi_{\theta p}}{\partial t}\right) + I_{p2}\left(\frac{\partial \phi_{\theta p}}{\partial t}\right)^2 + I_{p0}\left(\frac{\partial w_p}{\partial t}\right)^2 \end{array} \right\} (r + R_1) \mathrm{d}r \mathrm{d}\theta \tag{25}$$

$$I_{p0} = \sum_{k=1}^{N_L} \int_{Z_k}^{Z_{k+1}} \rho_p^k \mathrm{d}z$$

$$I_{p1} = \sum_{k=1}^{N_L} \int_{Z_k}^{Z_{k+1}} \rho_p^k \cdot z \mathrm{d}z \tag{26}$$

$$I_{p2} = \sum_{k=1}^{N_L} \int_{Z_k}^{Z_{k+1}} \rho_p^k \cdot z^2 \mathrm{d}z$$

$$T_{B_n} = \frac{1}{2} \int_0^{\vartheta} \left\{ \begin{array}{l} I_{bn0}\left(\frac{\partial u_{bn}}{\partial t}\right)^2 + 2I_{bn1}\left(\frac{\partial u_{bn}}{\partial t}\right)\left(\frac{\partial \phi_{xbn}}{\partial t}\right) + I_{bn2}\left(\frac{\partial \phi_{xbn}}{\partial t}\right)^2 + I_{bn0}\left(\frac{\partial v_{bn}}{\partial t}\right)^2 \\ \\ + 2I_{bn1}\left(\frac{\partial v_{bn}}{\partial t}\right)\left(\frac{\partial \phi_{\theta bn}}{\partial t}\right) + I_{bn2}\left(\frac{\partial \phi_{\theta bn}}{\partial t}\right)^2 + I_{bn0}\left(\frac{\partial w_{bn}}{\partial t}\right)^{2^2} \end{array} \right\} R_{bn} \mathrm{d}\theta_n \tag{27}$$

$$I_{bn0} = \sum_{k=1}^{N_L} \int_{Z_k}^{Z_{k+1}} \rho_{bn}^k dz_n,$$

$$I_{bn1} = \sum_{k=1}^{N_L} \int_{Z_k}^{Z_{k+1}} \rho_{bn}^k \cdot z_n dz_n, \tag{28}$$

$$I_{bn2} = \sum_{k=1}^{N_L} \int_{Z_k}^{Z_{k+1}} \rho_{bn}^k \cdot z_n^2 dz_n,$$

in which ρ_p^k is the material density of the k layer of the laminated plate, and ρ_{bn}^k represents the material density of the k layer of the laminated curved beam.

The specific expression of the total potential energy of laminated composite plates U_P and the total potential energy of nth laminated curved beam U_{B_n} are as follows:

$$U_P = U_{\text{stretch}} + U_{s-b} + U_{\text{bend}} = \frac{1}{2}\int_0^{R_P}\int_0^{\vartheta}\left\{\begin{array}{l} N_r^P\varepsilon_r^{p0} + N_r^P\varepsilon_r^{p0} + N_{r\theta}^P\gamma_{r\theta}^{p0} + M_r^P\chi_r^P \\ + M_\theta^P\chi_\theta^P + M_{r\theta}^P\chi_{r\theta}^P + Q_r^P\gamma_{rz}^{p0} + Q_\theta^P\gamma_{\theta z}^{p0}. \end{array}\right\} r\,\mathrm{d}r\mathrm{d}\theta \tag{29}$$

$$U_{\text{stretch}} = \frac{1}{2}\int_0^{R_P}\int_0^{\vartheta}\left\{\begin{array}{l} A_{11}\left(\dfrac{\partial u_p}{\partial r}\right)^2 + 2A_{12}\left(\dfrac{\partial v_p}{r\partial\theta} + \dfrac{u_p}{r}\right)\left(\dfrac{\partial u_p}{\partial r}\right) \\[3mm] + 2A_{16}\left(\dfrac{\partial v_p}{\partial r} + \dfrac{\partial u_p}{r\partial\theta} - \dfrac{v_p}{r}\right)\left(\dfrac{\partial u_p}{\partial r}\right) + A_{22}\left(\dfrac{\partial v_p}{r\partial\theta} + \dfrac{u_p}{r}\right)^2 \\[3mm] + 2A_{26}\left(\dfrac{\partial v_p}{r\partial\theta} + \dfrac{u_p}{r}\right)\left(\dfrac{\partial v_p}{\partial r} + \dfrac{\partial u_p}{r\partial\theta} - \dfrac{v_p}{r}\right) \\[3mm] + A_{66}\left(\dfrac{\partial v_p}{\partial r} + \dfrac{\partial u_p}{r\partial\theta} - \dfrac{v_p}{r}\right)^2 + \overline{\kappa}_s A_{44}\left(\dfrac{\partial w_p}{r\partial\theta} + \phi_{\theta p}\right)^2 \\[3mm] + 2\overline{\kappa}_s A_{45}\left(\dfrac{\partial w_p}{\partial r} + \phi_{rp}\right)\left(\dfrac{\partial w_p}{r\partial\theta} + \phi_{\theta p}\right) + \overline{\kappa}_s A_{55}\left(\dfrac{\partial w_p}{\partial r} + \phi_{rp}\right)^2 \end{array}\right\}(r+R_1)\mathrm{d}r\mathrm{d}\theta, \tag{30}$$

$$U_{s-b} = \int_0^{R_P}\int_0^{\vartheta}\left\{\begin{array}{l} B_{11}\left(\dfrac{\partial u_p}{\partial r}\right)\left(\dfrac{\partial\phi_{rp}}{\partial r}\right) + B_{12}\left(\dfrac{\partial\phi_{\theta p}}{r\partial\theta} + \dfrac{\phi_{rp}}{r}\right)\left(\dfrac{\partial u_p}{\partial r}\right) \\[3mm] + B_{16}\left(\dfrac{\partial\phi_{\theta p}}{\partial r} + \dfrac{\partial\phi_{rp}}{r\partial\theta} - \dfrac{\phi_{\theta p}}{r}\right)\left(\dfrac{\partial u_p}{\partial r}\right) + B_{12}\left(\dfrac{\partial\phi_{rp}}{\partial r}\right)\left(\dfrac{\partial v_p}{r\partial\theta} + \dfrac{u_p}{r}\right) \\[3mm] + B_{22}\left(\dfrac{\partial v_p}{r\partial\theta} + \dfrac{u_p}{r}\right)\left(\dfrac{\partial\phi_{\theta p}}{r\partial\theta} + \dfrac{\phi_{rp}}{r}\right) + B_{16}\left(\dfrac{\partial v_p}{\partial r} + \dfrac{\partial u_p}{r\partial\theta} - \dfrac{v_p}{r}\right)\left(\dfrac{\partial\phi_{rp}}{\partial r}\right) \\[3mm] + B_{26}\left(\dfrac{\partial v_p}{r\partial\theta} + \dfrac{u_p}{r}\right)\left(\dfrac{\partial\phi_{\theta p}}{\partial r} + \dfrac{\partial\phi_{rp}}{r\partial\theta} - \dfrac{\phi_{\theta p}}{r}\right) \\[3mm] + B_{26}\left(\dfrac{\partial v_p}{\partial r} + \dfrac{\partial u_p}{r\partial\theta} - \dfrac{v_p}{r}\right)\left(\dfrac{\partial\phi_{\theta p}}{r\partial\theta} + \dfrac{\phi_{rp}}{r}\right) \\[3mm] + B_{66}\left(\dfrac{\partial v_p}{\partial r} + \dfrac{\partial u_p}{r\partial\theta} - \dfrac{v_p}{r}\right)\left(\dfrac{\partial\phi_{\theta p}}{\partial r} + \dfrac{\partial\phi_{rp}}{r\partial\theta} - \dfrac{\phi_{\theta p}}{r}\right) \end{array}\right\}(r+R_1)\mathrm{d}r\mathrm{d}\theta \tag{31}$$

$$U_{\text{bend}} = \frac{1}{2}\int_0^{R_P}\int_0^{\vartheta}\left\{\begin{array}{l} D_{11}\left(\dfrac{\partial\phi_{rp}}{\partial r}\right)^2 + 2D_{12}\left(\dfrac{\partial\phi_{rp}}{\partial r}\right)\left(\dfrac{\partial\phi_{\theta p}}{r\partial\theta} + \dfrac{\phi_{rp}}{r}\right) \\[3mm] + 2D_{16}\left(\dfrac{\partial\phi_{rp}}{\partial r}\right)\left(\dfrac{\partial\phi_{\theta p}}{\partial r} + \dfrac{\partial\phi_{rp}}{r\partial\theta} - \dfrac{\phi_{\theta p}}{r}\right) + D_{22}\left(\dfrac{\partial\phi_{\theta p}}{r\partial\theta} + \dfrac{\phi_{rp}}{r}\right)^2 \\[3mm] + 2D_{26}\left(\dfrac{\partial\phi_{\theta p}}{r\partial\theta} + \dfrac{\phi_{rp}}{r}\right)\left(\dfrac{\partial\phi_{\theta p}}{\partial r} + \dfrac{\partial\phi_{rp}}{r\partial\theta} - \dfrac{\phi_{\theta p}}{r}\right) \\[3mm] + D_{66}\left(\dfrac{\partial\phi_{\theta p}}{\partial r} + \dfrac{\partial\phi_{rp}}{r\partial\theta} - \dfrac{\phi_{\theta p}}{r}\right)^2 \end{array}\right\}(r+R_1)\mathrm{d}r\mathrm{d}\theta \tag{32}$$

$$U_{\text{Bn}} = \frac{1}{2} \int_0^\vartheta \left\{ \begin{array}{l} A_{22}\left(\dfrac{\partial v_{\text{bn}}}{R_{\text{bn}}\partial\theta} + \dfrac{w_{\text{bn}}}{R_{\text{bn}}}\right)^2 + 2A_{26}\left(\dfrac{\partial u_{\text{bn}}}{R_{\text{bn}}\partial\theta}\right)\left(\dfrac{\partial v_{\text{bn}}}{R_{\text{bn}}\partial\theta} + \dfrac{w_{\text{bn}}}{R_{\text{bn}}}\right) + A_{66}\left(\dfrac{\partial u_{\text{bn}}}{R_{\text{bn}}\partial\theta}\right)^2 \\[4mm] + \overline{\kappa_s}A_{44}\left(\phi_{\text{xbn}}\right)^2 + 2\overline{\kappa_s}A_{45}\left(\dfrac{\partial w_{\text{bn}}}{R_{\text{bn}}\partial\theta} - \dfrac{v_{\text{bn}}}{R_{\text{bn}}} + \phi_{\text{bn}}\right)(\phi_{\text{xbn}}) \\[4mm] + \overline{\kappa_s}A_{55}\left(\dfrac{\partial w_{\text{bn}}}{R_{\text{bn}}\partial\theta} - \dfrac{v_{\text{bn}}}{R_{\text{bn}}} + \phi_{\theta\text{bn}}\right)^2 + 2B_{22}\left(\dfrac{\partial\phi_{\theta\text{bn}}}{R_{\text{bn}}\partial\theta}\right)\left(\dfrac{\partial v_{\text{bn}}}{R_{\text{bn}}\partial\theta} + \dfrac{w_{\text{bn}}}{R_{\text{bn}}}\right) \\[4mm] + 2B_{26}\left(\dfrac{\partial\phi_{\text{xbn}}}{R_{\text{bn}}\partial\theta}\right)\left(\dfrac{\partial v_{\text{bn}}}{R_{\text{bn}}\partial\theta} + \dfrac{w_{\text{bn}}}{R_{\text{bn}}}\right) + 2B_{26}\left(\dfrac{\partial\phi_{\theta\text{bn}}}{R_{\text{bn}}\partial\theta}\right)\left(\dfrac{\partial u_{\text{bn}}}{R_{\text{bn}}\partial\theta}\right) \\[4mm] + 2B_{66}\left(\dfrac{\partial\phi_{\text{xbn}}}{R_{\text{bn}}\partial\theta}\right)\left(\dfrac{\partial u_{\text{bn}}}{R_{\text{bn}}\partial\theta}\right) + D_{22}\left(\dfrac{\partial\phi_{\theta\text{bn}}}{R_{\text{bn}}\partial\theta}\right)^2 + D_{66}\left(\dfrac{\partial\phi_{\text{xbn}}}{R_{\text{bn}}\partial\theta}\right)^2 \\[4mm] + 2D_{26}\left(\dfrac{\partial\phi_{\text{xbn}}}{R_{\text{bn}}\partial\theta}\right)\left(\dfrac{\partial\phi_{\theta\text{bn}}}{R_{\text{bn}}\partial\theta}\right) \end{array} \right\} R_{\text{bn}}\mathrm{d}\theta_n, \tag{33}$$

In the equation, the total potential energy of the composite-laminated rotationally stiffened plate U_{P} includes tensile potential energy U_{stretch}, bowing potential energy U_{bend}, tensile and bowing potential energy coupling $U_{\text{s–b}}$, and the expressions are also been given.

As the boundary conditions of the laminated plate in the composite-laminated rotationally stiffened plate model established in this paper are determined by the boundary spring set, the potential energy of the boundary spring U_{SP} will be generated, and its specific expression is as follows:

$$U_{\text{SP}} = U_{\text{SP}}^\theta + U_{\text{SP}}^s, \tag{34}$$

$$U_{\text{SP}}^\theta = \frac{1}{2} \int_0^\vartheta \int_{-h_\text{p}/2}^{h_\text{p}/2} \left\{ \begin{array}{l} \left[k_{r0}^u u_\text{p}^2 + k_{r0}^v v_\text{p}^2 + k_{r0}^w w_\text{p}^2 + K_{r0}^r \phi_{r\text{p}}^2 + K_{r0}^\theta \phi_{\theta\text{p}}^2\right]_{r=0} \\[2mm] + \left[k_{rR_\text{p}}^u u_\text{p}^2 + k_{rR_\text{p}}^v v_\text{p}^2 + k_{rR_\text{p}}^w w_\text{p}^2 + K_{rR_\text{p}}^r \phi_{r\text{p}}^2 + K_{rR_\text{p}}^\theta \phi_{\theta\text{p}}^2\right]_{r=R_\text{p}} \end{array} \right\} (r + R_1)\mathrm{d}z\mathrm{d}\theta, \tag{35}$$

$$U_{\text{SP}}^s = \frac{1}{2} \int_0^{R_\text{p}} \int_{-h_\text{p}/2}^{h_\text{p}/2} \left\{ \begin{array}{l} \left[k_{\theta0}^u u_\text{p}^2 + k_{\theta0}^v v_\text{p}^2 + k_{\theta0}^w w_\text{p}^2 + K_{\theta0}^r \phi_{r\text{p}}^2 + K_{\theta0}^\theta \phi_{\theta\text{p}}^2\right]_{\theta=0} \\[2mm] + \left[k_{\theta\vartheta}^u u_\text{p}^2 + k_{\theta\vartheta}^v v_\text{p}^2 + k_{\theta\vartheta}^w w_\text{p}^2 + K_{\theta\vartheta}^r \phi_{r\text{p}}^2 + K_{\theta\vartheta}^\theta \phi_{\theta\text{p}}^2\right]_{\theta=\vartheta} \end{array} \right\} \mathrm{d}z\mathrm{d}r. \tag{36}$$

For composite-laminated rotationally stiffened plate, the analysis of the coupled potential $U_{P-\text{coupling}}$ and $U_{B_n-\text{coupling}}$ of the laminated plate and the laminated beam will be different due to the different sizes of the rotation angle ϑ; when $0 < \vartheta < 360°$, since the left and right sides of the stiffened plate rotation are not coupled, there is no coupled potential of the laminated plate and laminated beam, and

when $\vartheta = 360°$, the left and right sides of the stiffened plate rotation are coupled, producing coupled potential at this time.

When $\vartheta = 360°$, the coupled potential of the laminated plate in the stiffened plate $U_{P-\text{coupling}}$ and the coupled potential of the nth laminated curved beam in the stiffened plate $U_{B_n-\text{coupling}}$ can be written as follows:

$$U_{P-\text{coupling}} = \frac{1}{2} \int_0^{R_p} \int_{-h_p/2}^{h_p/2} \left\{ \begin{array}{c} k_{uc}^p \left(u_p|_{\theta=360°} - u_p|_{\theta=0}\right)^2 + k_{vc}^p \left(v_p|_{\theta=360°} - v_p|_{\theta=0}\right)^2 \\ + k_{wc}^p \left(w_p|_{\theta=360°} - w_p|_{\theta=0}\right)^2 + K_{rc}^p \left(\phi_{rp}|_{\theta=360°} - \phi_{rp}|_{\theta=0}\right)^2 \\ + K_{\theta c}^p \left(\phi_{\theta p}|_{\theta=360°} - \phi_{\theta p}|_{\theta=0}\right)^2 \end{array} \right\} dz dr, \tag{37}$$

$$U_{B_n-\text{coupling}} = \frac{1}{2} \int_0^{\vartheta} \int_{-h_n/2}^{h_n/2} \left\{ \begin{array}{c} k_{uc}^{bn} \left(u_{bn}|_{\theta_n=360°} - u_{bn}|_{\theta_n=0}\right)^2 + k_{vc}^{bn} \left(v_{bn}|_{\theta_n=360°} - v_{bn}|_{\theta_n=0}\right)^2 \\ + k_{wc}^{bn} \left(w_{bn}|_{\theta_n=360°} - w_{bn}|_{\theta_n=0}\right)^2 + K_{xc}^{bn} \left(\phi_{xbn}|_{\theta_n=360°} - \phi_{xbn}|_{\theta_n=0}\right)^2 \\ + K_{\theta c}^{bn} \left(\phi_{\theta bn}|_{\theta_n=360°} - \phi_{\theta bn}|_{\theta_n=0}\right)^2 \end{array} \right\} dz_n. \tag{38}$$

The coupled potential generated by the coupling of the laminated plate and the nth laminated curved beam $W_{P\&B_n}$ can be expressed as follows:

$$W_{P\&B_n} = \frac{1}{2} \int_0^{\vartheta} \left\{ \begin{array}{c} k_{uc}^{cp} \left(u_p|_{r=R_b} - w_{bn}\right)^2 + k_{vc}^{cp} \left(v_p|_{r=R_b} - v_{bn}\right)^2 + k_{wc}^{cp} \left(w_p|_{r=R_b} - u_{bn}\right)^2 \\ + K_{xc}^{cp} \left(\phi_{rp}|_{r=R_b} - \phi_{xbn}\right)^2 + K_{yc}^{cp} \left(\phi_{\theta p}|_{r=R_b} - \phi_{\theta bn}\right)^2 \end{array} \right\} d\theta. \tag{39}$$

The specific expression of the work W_F done by the simple harmonic point force F on the laminated plate of stiffened composite plate is as follows:

$$W_F = \iint_S \left\{ f_u u_p + f_v v_p + f_w w_p + f_{\phi_r} \phi_{rp} + f_{\phi_\theta} \phi_{\theta p} \right\} r dr d\theta, \tag{40}$$

$$f_i = F\delta(r - r_0)\delta(\theta - \theta_0), \tag{41}$$

where f_i ($i = u_j, v_j, w_j, \phi_r, \phi_\theta$) is a function of external load distribution, and the location of simple harmonic point force F is (r_0, θ_0).

After obtaining the energy equation of the composite-laminated rotationally stiffened plate, each energy equation is substituted into the Lagrange equation (21) and (22). According to the Rayleigh–Ritz method [21], calculating the partial derivative of the two-dimensional and one-dimensional unknown Fourier coefficients in the Lagrange equation and making the result equal to zero, we can get

$$\frac{\partial L_P}{\partial \mathbf{P}_{mn}} = \frac{\partial T_P}{\partial \mathbf{P}_{mn}} - \frac{\partial U_P}{\partial \mathbf{P}_{mn}} - \frac{\partial U_{P-\text{coupling}}}{\partial \mathbf{P}_{mn}} - \frac{\partial U_{SP}}{\partial \mathbf{P}_{mn}} - \frac{\partial W_{P\&B_n}}{\partial \mathbf{P}_{mn}} + \frac{\partial W_F}{\partial \mathbf{P}_{mn}} = \mathbf{0}, \tag{42}$$

$$\frac{\partial L_{B_n}}{\partial \mathbf{Q}_l} = \frac{\partial T_{B_n}}{\partial \mathbf{Q}_l} - \frac{\partial U_{B_n}}{\partial \mathbf{Q}_l} - \frac{\partial U_{B_n-\text{coupling}}}{\partial \mathbf{Q}_l} - \frac{\partial W_{P\&B_n}}{\partial \mathbf{Q}_l} = \mathbf{0}, \tag{43}$$

$$\mathbf{P}_{mn} = \begin{bmatrix} \mathbf{A}_{mn} & \mathbf{B}_{mn} & \mathbf{C}_{mn} & \mathbf{D}_{mn} & \mathbf{E}_{mn} \end{bmatrix}^T, \tag{44}$$

$$\mathbf{Q}_l = \begin{bmatrix} \mathbf{A}_l & \mathbf{B}_l & \mathbf{C}_l & \mathbf{D}_l & \mathbf{E}_l \end{bmatrix}^T, \tag{45}$$

in which $\mathbf{P}_{mn}$ is the unknown two-dimensional Fourier coefficient matrix of the laminated plate, and $\mathbf{Q}_l$ is the unknown one-dimensional Fourier coefficient matrix of the laminated curved beam.

Convert equations (40)–(43) into the matrix form as follows:

$$\left(\mathbf{K}_P - \omega^2 \mathbf{M}_P\right)\mathbf{P}_{mn} + \mathbf{C}_{B_n \& P}\mathbf{Q}_l = \mathbf{F}, \tag{46}$$

$$\left(\mathbf{K}_{B_n} - \omega^2 \mathbf{M}_{B_n}\right)\mathbf{Q}_l + \omega^2 \mathbf{C}_{P \& B_n}\mathbf{P}_{mn} = \mathbf{0}, \tag{47}$$

where $\mathbf{K}_P$ and $\mathbf{K}_{B_n}$, respectively, represent the stiffness matrix of the laminated plate and the nth laminated curved beam in the composite laminated rotationally stiffened plate; $\mathbf{M}_P$ and $\mathbf{M}_{B_n}$ are the mass matrix of the laminated plate and the nth laminated curved beam; $\mathbf{C}_{B_n \& P}$ represents the coupling matrix between the nth laminated curved beam and the laminated plate of the stiffened plate, and $\mathbf{C}_{P \& B_n} = \mathbf{C}_{B_n \& P}{}^T$.

When F is 0, the equations for solving the natural frequencies and modes of composite laminated rotationally stiffened plates can be obtained by combining equations (44) and (45). At this time, direct calculation belongs to the nonlinear solution, so it needs to be converted into linear equations to be solved. The results after conversion are as follows:

$$\left(\mathbf{R} - \omega^2 \mathbf{S}\right)\mathbf{G} = \mathbf{0}, \tag{48}$$

$$\mathbf{R} = \begin{pmatrix} \mathbf{K}_P & \mathbf{C}_{B_n \& P} \\ 0 & \mathbf{K}_{B_n} \end{pmatrix}, \tag{49}$$

$$\mathbf{S} = \begin{pmatrix} \mathbf{M}_P & 0 \\ -\mathbf{C}_{P \& B_n} & \mathbf{M}_{B_n} \end{pmatrix}, \tag{50}$$

$$\mathbf{G} = \begin{pmatrix} \mathbf{P}_{mn} \\ \mathbf{Q}_l \end{pmatrix}. \tag{51}$$

Finally obtained characteristic solution ω is the natural frequency of the composite-laminated rotationally stiffened plate, and the eigenvector $\mathbf{G}$ is its corresponding mode. By substituting the simple harmonic point force into equations (46)–(48), the steady-state response of the stiffened plate can be obtained.

3. Numerical Results and Discussion

According to the unified analysis model of composite-laminated rotationally stiffened plates established in Section 2.2, this section has carried out numerical discussion and result analysis on the selected part of the calculation to further study the vibration characteristics of stiffened annular sector plates, circular sector plates, annular plates, and circular plates under different dimensions and material parameters, mainly including the following two parts: (1) convergence and correctness verification and (2) the influence of related parameters on the vibration characteristics of composite-laminated rotationally stiffened plates under free vibration. Due to the lack of research on composite-laminated rotationally stiffened plates, few literature parameters can be found for comparison, so the results of the calculation of this section are compared with the results of the experiment and finite element simulation results.

Table 1 shows the material parameters used for laminated plates and laminated curved beams in this section. The dimensionless natural frequency parameter is defined as $\Omega = \omega / h_p \sqrt{\rho / E_1}$. The four boundary conditions of free, simply supported, fixed supported, and elastic in this section are simplified and described as F, S, C, and E, respectively. According to the difference of stiffened annular sector plate, circular sector plate, annular plate, and circular plate, there are four ways of expression: (1) stiffened annular sector plate structure: FSCE indicates $\theta = 0$, $\theta = \vartheta$, $r = 0$, and $r = R_p$ are free, simply supported, fixed supported, and elastic boundaries, respectively; (2) stiffened circular sector plate structure: FSC indicates $\theta = 0$, $\theta = \vartheta$, and $r = R_p$ are free, simply supported, and fixed supported boundary, respectively; (3) stiffened annular plate structure: FS indicates $r = 0$ and $r = R_p$ are free and simply supported boundary, respectively; and (4) stiffened circular plate structure: S indicates $r = R_p$ is a simply supported boundary.

3.1. Model Validation. This section will verify the convergence and correctness of the model of composite-laminated rotationally stiffened plate established in Section 2.2, including the convergence of natural frequency cutoff value and spring stiffness value. As mentioned in the previous chapters, the admissible displacement function of stiffened plates in this paper is expressed as improved Fourier series expansion. Therefore, in the process of solving the energy equation including the admissible displacement function, the calculation results may not converge, so it is necessary to verify the convergence of the established analysis model. At the same time, the number of expanded items in the expansion also needs to be analyzed. Theoretically, the more terms the expansion term has, the higher the accuracy of the solution of the equation will be. However, the number of expansion terms can meet the requirement of solving accuracy. Further increasing the number of expansion terms will not significantly improve the solving accuracy but reduce the solving efficiency. Therefore, it is necessary to confirm the cutoff value of the admissible displacement function of the stiffened plate. The cutoff value of the laminated plate is M_p, N_p, and the cutoff value of the laminated curved beam is M_b.

Table 2 shows the first eight natural frequencies of stiffened plates under different cutoff values of laminated plates and laminated curved beams obtained by this method and compares them with the finite element simulation results. The stiffened plate model is a unified model, which can theoretically calculate the natural frequency of any size of rotational stiffened composite plate; in this example, the geometric parameters of composite-laminated rotationally stiffened plates have been determined as follows: $R_2 = 2\,\text{m}$, $b_1 = 0.06\,\text{m}$, and $h_1 = 0.04\,\text{m}$. The material of the laminated plate is graphite fiber resin, and the angle-ply is [0°/90°]. The number of laminated plated curved beams is 1, located at $R_p/2$, and the material is steel. It is not difficult to see from Table 2 that when $M_p \times N_p$ is 18×18 and M_b is 50, the natural frequencies of each order basically converged. The size and coordinate system used in the finite element model

Table 1: Material parameters used in the numerical calculations in this section for laminated plates and laminated curved beams.

Material	ρ (kg/m³)	Material property parameters					
		E_1 (Pa)	E_2 (Pa)	G_{23} (Pa)	G_{12} (Pa)	G_{13} (Pa)	μ_{12}
Graphite fiber resin	1600	1.85×10^{11}	1.09×10^{10}	7.3×10^9	7.3×10^9	7.3×10^9	0.28
Glass epoxy resin	1810	3.9×10^{10}	8.4×10^9	4.2×10^{10}	4.2×10^{10}	4.2×10^{10}	0.26
Q235 steel	7800	2.16×10^{11}	2.16×10^{11}	8.31×10^{10}	8.31×10^{10}	8.31×10^{10}	0.3

are the same as that of the model established in this paper, the mesh size is 0.02 of the global size, and the element shape of the sound cavity is AC3D20:20 node acoustic quadric hexahedron element. The shape of the composite structural element is C3D20R: twenty-node hexahedron element. By referring to the results of finite element simulation, the maximum error between the natural frequencies of each order and the results of finite element simulation is 6.38%. Therefore, the cutoff value is determined as $M_p \times N_p = 18 \times 18$ and $M_b = 50$ in the numerical calculation later in this paper.

It is not difficult to see from Table 2 that the cutoff value of the laminated curved beam has little influence on the convergence of the analytical model. Therefore, Figure 3 only shows the change curve of some order natural frequency parameter Ω of the composite-laminated rotationally stiffened plate under different cutoff values of the laminated plate (where $M_p = N_p$). As shown in Figure 3, the natural frequency parameter Ω of the four stiffened plate structures tends to be stable with the increase of the cutoff value, which more intuitively reflects the convergence of the present analysis model.

To have a more intuitive understanding of the modes obtained by this method, Figure 4 shows the modal shapes diagram of four types of composite-laminated rotationally stiffened plate structures obtained by this method and the finite element method (FEM). The material parameters and dimension parameters of the four stiffened plate structures are the same as those in Table 2. It can be found that the modal diagrams obtained by the present method are completely corresponding to the results of the finite element method.

In this chapter, artificial virtual spring technology is used to simulate the boundary conditions and coupling conditions of the model. The change of the boundary and coupling conditions of the composite-laminated rotationally stiffened plate is realized by changing the boundary and coupling spring stiffness value. For boundary or coupling conditions that require rigid fixation, the spring stiffness value should be set to a larger value. However, due to the limitation of the algorithm, the spring stiffness value cannot be infinite in actual calculation. Therefore, to facilitate the follow-up research, it is necessary to select a reasonable spring stiffness value to simulate the rigidly fixed boundary or coupling conditions and verify its convergence. Since the stiffener in the composite-laminated rotationally stiffened plate does not need to set the boundary conditions, the effect of boundary spring stiffness value can be analyzed only for the structure of the rotationally composite plate. The specific scope includes linear spring $k(k_u, k_v, k_w)$, torsion spring

$K(K_r, K_\theta)$, intraplate coupling spring kc $(k_{uc}^p, k_{vc}^p, k_{wc}^p, k_{rc}^p, k_{\theta c}^p)$, and plate-beam coupling spring kcp $(k_{uc}^{cp}, k_{vc}^{cp}, k_{wc}^{cp}, k_{xc}^{cp}, k_{xc}^{cp}, k_{yc}^{cp})$.

Taking the annular sector plate as an example, the influence of the boundary spring stiffness value is analyzed. The change curve of the first four frequency parameters under different boundary spring stiffness values is shown in Figure 5. The material parameters and size parameters of the plate structure are the same as those in Table 2. It is not difficult to see from Figure 5(a) that the stiffness value k of the linear boundary spring is in the range of 10^{-4}–10^1, and the values of the first four frequency parameters are stable and close to 0. It can be considered that the boundary condition of the annular sector plate can be regarded as a free boundary at this time. When the linear spring stiffness value k is analyzed, the torsion spring stiffness value K is automatically set to zero. With the increase of the linear spring stiffness, the frequency parameters of the annular sector plate also continue to increase and tend to be stable in the range of 10^{10}–10^{16}. At this time, the boundary condition of the annular sector plate can be regarded as a simply supported boundary. In Figure 5(b), the linear boundary spring stiffness value is always kept at 10^{16}. With the increase of the torsion spring stiffness value, the frequency parameter of the annular sector plate also continues to increase and tends to be stable in the range of 10^7–10^{16}. At this time, the boundary condition of the annular sector plate can be regarded as a fixed support boundary. According to the abovementioned conclusions, the value of boundary spring stiffness under different boundary conditions is shown in Table 3, the classical boundary conditions of free, simply supported, clamped supported are simplified as F, S, C respectively. The spring stiffness value can be given arbitrarily under the elastic boundary condition. This paper gives an example which is marked with E. In the numerical calculation in this chapter, the spring stiffness values of various boundary conditions are based on those in Table 3. The numerical calculation of the spring stiffness values of various boundary conditions in this paper is based on Table 3.

The study of the coupling condition of the interior of the plate is similar to the boundary conditions. Taking the annular plate as an example, Figure 6 shows the frequency parameter change curve of the order of the annular plate with different coupling spring stiffness values of the interior of the plate under the two boundary conditions. The material parameters and dimension parameters of the annular plate are the same as those in Table 2. It can be seen from Figure 6 that when the stiffness value kc of the coupling spring in the plate is less than 10^4, the frequency parameters of the corresponding part of the order remain stable and less than

TABLE 2: Convergence analysis of the frequency parameter Ω for composite-laminated rotationally stiffened plates.

$M_p \times N_p$	M_b	Order modal							
		1	2	3	4	5	6	7	8
Stiffened annular sector plate: $R_1 = 0.5$m, $h_p = 0.01$m, $R_{b1} = 1.25$m, $\vartheta = 90°$, CCCC									
6×6	25	2.537	5.040	5.705	6.562	6.989	8.047	8.378	11.636
	50	2.537	5.040	6.005	6.862	6.989	8.046	8.377	11.636
10×10	25	2.535	4.914	5.459	5.939	6.474	7.499	7.746	9.147
	50	2.535	4.914	5.459	5.939	6.474	7.499	7.746	9.147
14×14	25	2.534	4.866	5.376	5.744	6.377	7.387	7.592	8.994
	50	2.534	4.866	5.376	5.744	6.377	7.387	7.592	8.994
18×18	25	2.533	4.837	5.332	5.654	6.331	7.343	7.521	8.943
	50	2.533	4.837	5.332	5.654	6.331	7.343	7.521	8.943
	FEM	2.559	5.098	5.268	5.579	6.304	7.547	7.646	9.194
Stiffened circular sector plate: $R_1 = 0$m, $h_p = 0.01$m, $R_{b1} = 1$m, $\vartheta = 90°$, CCC									
6×6	25	2.532	3.895	4.153	5.308	6.929	7.277	8.648	11.522
	50	2.532	3.895	4.153	5.308	6.929	7.277	8.648	11.521
10×10	25	2.406	3.699	3.964	4.725	6.303	6.723	8.392	9.064
	50	2.406	3.699	3.964	4.725	6.303	6.723	8.392	9.064
14×14	25	2.335	3.642	3.947	4.657	6.214	6.575	8.253	8.692
	50	2.335	3.642	3.947	4.657	6.214	6.575	8.253	8.692
18×18	25	2.288	3.617	3.937	4.632	6.189	6.511	8.219	8.549
	50	2.288	3.617	3.937	4.632	6.189	6.511	8.219	8.549
	FEM	2.332	3.634	3.835	4.789	6.190	6.371	8.145	8.397
Stiffened annular plate: $R_1 = 0.5$m, $h_p = 0.04$m, $R_{b1} = 1.25$m, $\vartheta = 360°$, CC									
6×6	25	0.963	1.161	1.161	1.285	1.286	1.601	1.601	2.178
	50	0.963	1.161	1.161	1.285	1.286	1.601	1.601	2.178
10×10	25	0.959	1.158	1.158	1.280	1.280	1.565	1.568	2.178
	50	0.959	1.158	1.158	1.280	1.280	1.565	1.568	2.178
14×14	25	0.959	1.157	1.157	1.278	1.278	1.562	1.562	2.177
	50	0.959	1.157	1.157	1.278	1.278	1.562	1.562	2.177
18×18	25	0.959	1.157	1.157	1.277	1.277	1.560	1.560	2.176
	50	0.959	1.157	1.157	1.277	1.277	1.560	1.560	2.176
	FEM	0.988	1.029	1.029	1.155	1.252	1.576	1.577	2.160
Stiffened circular plate: $R_1 = 0$m, $h_p = 0.1$m, $R_{b1} = 1$m, $\vartheta = 360°$, C									
6×6	25	0.325	0.633	0.633	0.971	0.972	1.217	1.413	1.416
	50	0.325	0.633	0.633	0.971	0.972	1.217	1.404	1.405
10×10	25	0.324	0.632	0.632	0.969	0.969	1.217	1.381	1.383
	50	0.324	0.632	0.632	0.969	0.969	1.217	1.381	1.383
14×14	25	0.324	0.632	0.632	0.969	0.969	1.217	1.381	1.381
	50	0.324	0.632	0.632	0.969	0.969	1.217	1.381	1.381
18×18	25	0.324	0.632	0.632	0.969	0.969	1.216	1.381	1.381
	50	0.324	0.632	0.632	0.969	0.969	1.216	1.381	1.381
	FEM	0.308	0.609	0.610	0.955	1.035	1.150	1.455	1.468

the frequency parameters when the stiffness value kc is larger; therefore, it can be considered that the coupling spring within this range has limited influence on the frequency parameters of the annular plate structure. With the increase of the stiffness value kc of the coupling spring in the plate, the frequency parameter of the annular plate also increases. When the stiffness value kc increases to 10^8, the frequency parameters of the annular plate also tend to be stable. From the abovementioned phenomena, it can be seen that when the stiffness value of the coupling spring in the plate reaches 10^8, the rigid coupling of the coupling boundary of the rotary composite plate can be realized. To ensure the correctness of the calculation results, the stiffness

value kc of the coupled spring in the plate was set as 10^{16} in the subsequent example.

To study the coupling conditions of plate and beam, it is necessary to take the rotational stiffened composite plate as an example. This example selects the composite-stiffened annular sector plate with the same material parameters and size parameters as those in Table 2. Figure 7 shows the frequency parameter change curve of the partial order of the stiffness value of the coupling spring of different plates and beams under two boundary conditions. It is not difficult to see that the effect of the plate-beam coupling spring stiffness value kcp on the frequency parameter Ω is similar to the interior of a plate coupling spring stiffness value kc. When
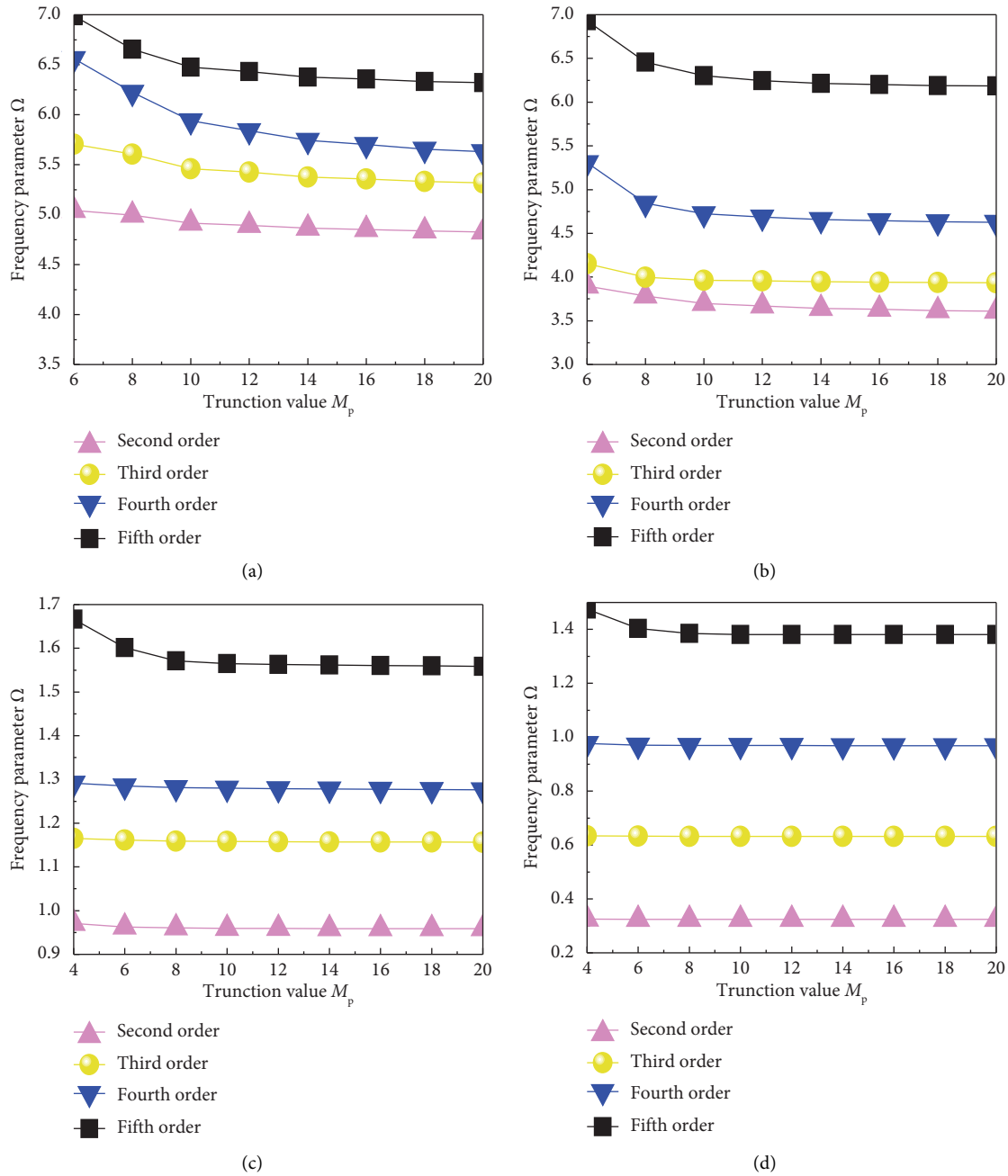
FIGURE 3: Variation curve of natural frequency parameter Ω of the composite-laminated rotationally stiffened plate under different cutoff values. (a) Stiffened annular sector plate. (b) Stiffened circular sector plate. (c) Stiffened annular plate. (d) Stiffened circular plate.

the stiffness value kcp is less than 10^4, the plate-beam coupling spring hardly plays the role of coupling between plates and beams in this range and has limited influence on the frequency parameter Ω. When the stiffness value kcp increases to 10^{10}, the rigid coupling of the coupling boundary between the rotary composite plate and the laminated beam can be realized.

In this section, the frequency response function method is used to carry out the structural modal test of a stiffened circular plate with a fixed support boundary, and the test results are compared with the results of this method to verify

the accuracy of the model of the stiffened composite plate of revolution established by this method. The test instruments include the LC02 force hammer, 3A105 force sensor, DH5857-1 charge adjuster, 1A116E acceleration sensor, and DH5922D dynamic signal test and analysis system. The single point pickup method is adopted when collecting data. The position of the sensor remains unchanged, and a force hammer is used to knock the intersection point of the grid drawn before. After hitting all the test points set, the peak position of the frequency response curve drawn is determined in the test software according to the collected data,

Stiffened annular sector plate:
Present method

| First order | Second order | Third order | Fourth order |

FEM

| First order | Second order | Third order | Fourth order |

Stiffened circular sector plate:
Present method

| First order | Second order | Third order | Fourth order |

FEM

| First order | Second order | Third order | Fourth order |

Stiffened annular plate:
Present method

| First order | Second order | Third order | Fourth order |

FEM

| First order | Second order | Third order | Fourth order |

Stiffened circular plate:
Present method

| First order | Second order | Third order | Fourth order |

FEM

| First order | Second order | Third order | Fourth order |

FIGURE 4: Modal shape diagram of the composite-laminated rotationally stiffened plate structure.

which is the natural frequency of the test stiffened plate. By calculating the mode in the test software, the relevant mode can be obtained.

Figure 8 shows the stiffened circular plate under the fixed support boundary condition. Thrity-two Φ16 bolts arranged uniformly along the circumference are tightly connected with the upper and lower splints to form the fixed support boundary condition. The structural dimension parameters of the stiffened plate used in the stiffened circular plate test are

$R_1 = 0$ m, $R_2 = 0.265$ m, $h_p = 0.005$ m, $R_{b1} = 0.088$ m, $R_{b2} = 0.177$ m, $b_1 = b_2 = 0.02$ m, $h_1 = h_2 = 0.01$ m, and $\vartheta = 360°$. The material of the stiffened circular plate includes Q235 steel and carbon fiber composite material, the material parameter of the Q235 steel is $E = 216$ GPa, $\mu = 0.3$, and $\rho_p = 7800$ kg/m³. The material parameters of carbon fiber composite material are $E_1 = E_2 = 77.8$ GPa, $G_1 = G_2 = G_3 = 77.8$ GPa, $\mu = 0.26$, and $\rho_p = 7800$ kg/m³; and the layer angle is [0°/90°/0°/90°/0°].

(a)

(b)
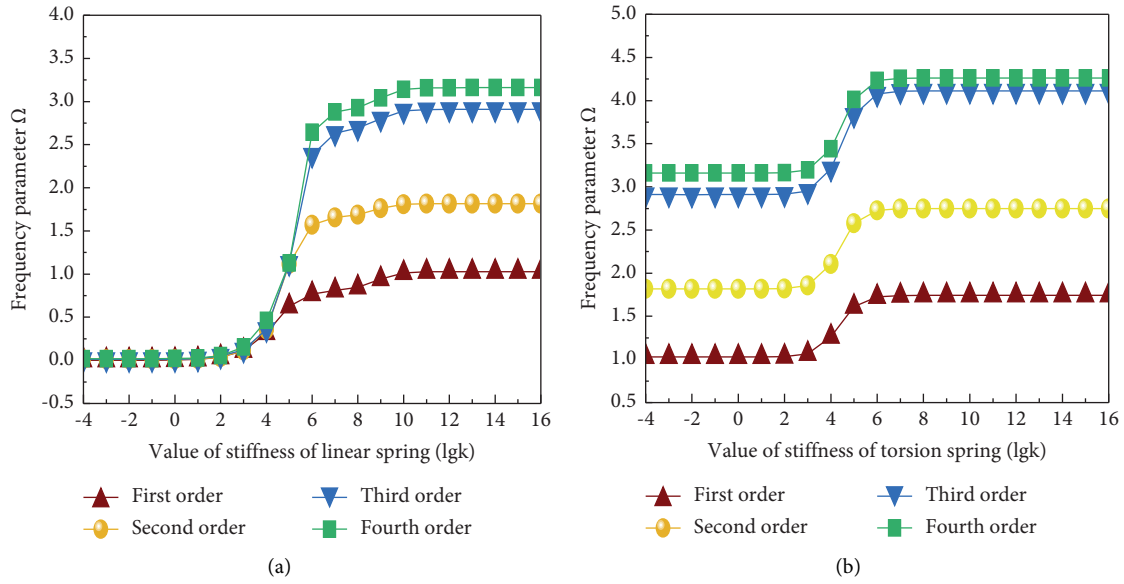
Figure 5: Variation curve of frequency parameter Ω of composite annular sector plate under different values of boundary spring stiffness. (a) Value of linear spring stiffness. (b) Value of torsion spring stiffness.

Table 3: Value of boundary spring stiffness under different boundary conditions.

Boundary condition	Value of boundary spring stiffness				
	k_u	k_v	k_w	K_r	K_θ
C	10^{16}	10^{16}	10^{16}	10^{16}	10^{16}
S	10^{16}	10^{16}	10^{16}	0	0
F	0	0	0	0	0
E	10^6	10^6	10^6	0	0

(a)

(b)
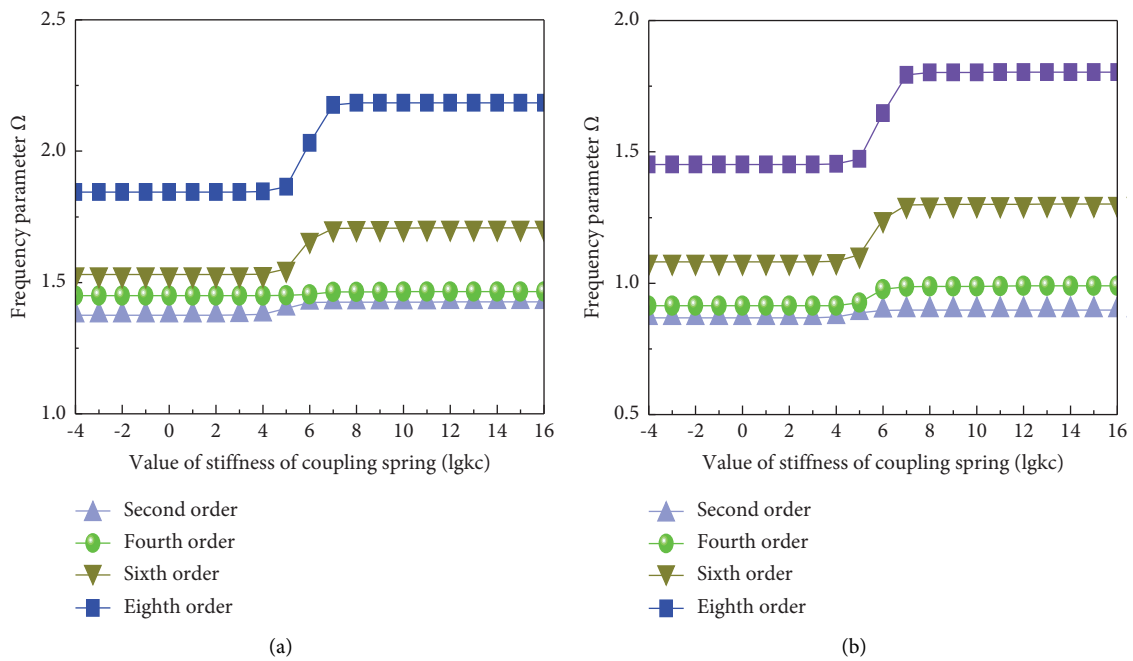
Figure 6: Variation curve of frequency parameter Ω of the composite annular plate under different values of coupling spring stiffness. (a) Boundary condition CC. (b) Boundary condition SS.

(a)

(b)
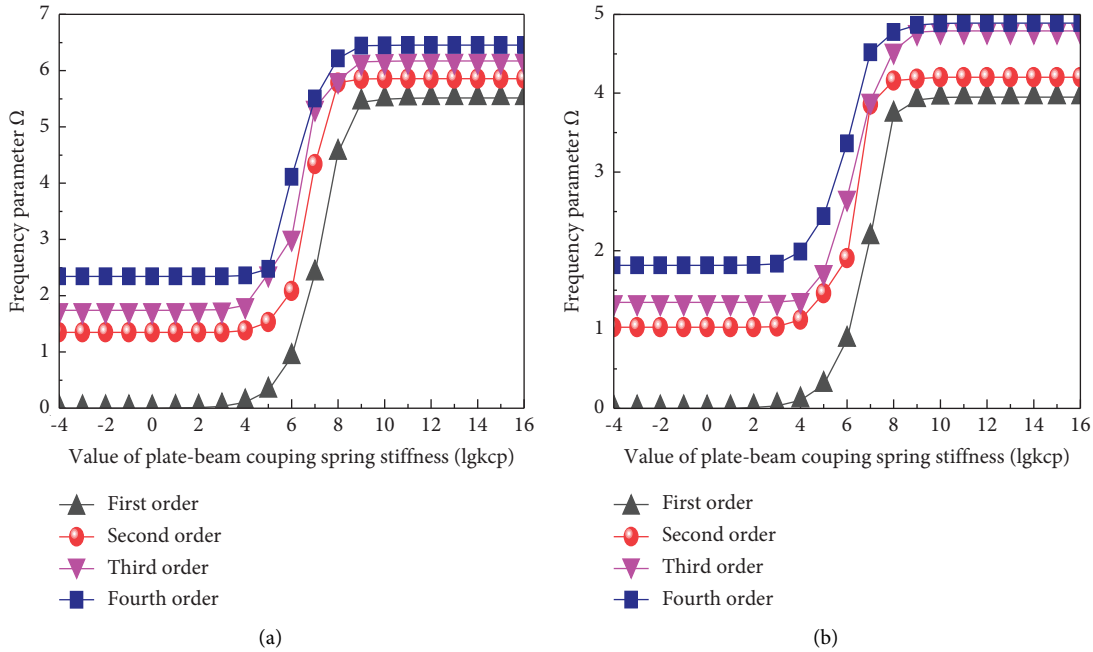
FIGURE 7: Variation curve of frequency parameters Ω of composite-stiffened annular sector plate under different values of plate-beam coupling spring stiffness. (a) Boundary condition CCCC. (b) Boundary condition SSSS.

(a)

(b)

FIGURE 8: Stiffened circular sector plate under the fixed boundary condition. (a) Q235 steel. (b) Carbon fiber composite material.

Figure 9 shows the layout of the stiffened circular plate structure and test equipment during the real test. Before the test, the stiffened circular plate structure was divided into units. The specific division method was as follows: 4 equal divisions were conducted in the r direction and 12 equal divisions in the θ direction. There were 49 measuring points in total, and the acceleration sensor was located at 22 measuring points. Figure 10 shows the natural frequencies and modal shapes of the partial orders of stiffened circular plates of Q235 steel and carbon fiber composite material obtained from the test and the method in this paper. From the contents of Figure 10, when stiffened circular plates are made of Q235 steel, it is not difficult to find that the maximum error between the test results and the calculation results of this method is 7.56%, and when stiffened circular plates are made of carbon fiber composite material, it is not difficult to find that the

maximum error between the test results and the calculation results of this method is 3.18% while the experimental results correspond with the modal shapes obtained by this method, The deviation of the abovementioned experimental results is within the acceptable range, which fully proves the correctness of the analysis model. The experimental error is caused by many reasons. First of all, the fixed boundary conditions of the plate cannot be fully simulated by the way of clamping the foundation frame and the battens. Then, the material parameters used in the numerical calculation of the plate deviate from the actual material parameters of the work piece, and the work piece cannot be completely ideal isotropic material. In addition, the accuracy deviation of the force sensor and acceleration sensor and the human error of the experimenter in the process of hammering will cause the error of experimental data.

Figure 9: Layout plan of stiffened circular sector plate structure and test equipment.

3.2. Free Vibration Analysis. After verifying the convergence and correctness of the unified analysis model of composite-laminated rotationally stiffened plates, this section will analyze the free vibration of composite-laminated rotationally stiffened plates according to the model of composite-laminated rotationally stiffened plates and study the influence of various relevant parameters on the vibration characteristics of stiffened plates.

In the theoretical modeling in the previous section, it has been mentioned that the composite-laminated rotationally stiffened plate is composed of the rotary composite plate structure and the rotary composite-laminated curved beam in the theoretical modeling in the previous section. The influence of the parameters of the rotationally composite plate structure on the vibration characteristics of the stiffened plate structure is analyzed here. The frequency parameters of composite-laminated rotationally stiffened plates with different plate structure parameters are obtained by the method in this paper. Taking the stiffened circular sector plate as an example, the calculation results are shown in Table 4. The stiffened plate in this example has two laminated curved beams as stiffeners, of which stiffener 1 is at $R_p/2$ and stiffener 2 is at $R_p/3$. The material of the laminated plate and laminated curved beam is glass epoxy resin, and the layer angle is the same. The fixed geometric parameters in the calculation example are $R_1 = 0$ m, $R_2 = 1.5$ m, $h_p = 0.02$ m, $R_{b1} = 0.75$ m, $R_{b2} = 0.5$ m, $b_1 = b_2 = 0.08$ m, and $h_1 = h_2 = 0.05$ m. It can be seen from Table 4 that the boundary conditions, angle-ply, and rotation angle all have an impact on the frequency parameter Ω of composite-laminated rotationally stiffened plates.

To further analyze the influence of boundary and parameter conditions on the vibration characteristics of composite-laminated rotationally stiffened plates, the parametric study of relevant conditions is also carried out in the form of curves. Take the stiffened circular sector plate in Table 4 as an example, Figure 11 shows the changing curve of the first four frequency parameters Ω with rotation angle ϑ under different boundary conditions ϑ, which reflects the influence of boundary conditions and rotation angle ϑ on the frequency parameter Ω. The angle-ply of the stiffened composite circular sector plate selected in the calculation example is [90°/0°/90°]. It can be seen from Figure 11 that the frequency parameter Ω of stiffened composite circular sector-stiffened plate decreases with the increase of rotation angle ϑ, and the larger the rotation angle ϑ is, the smaller the decreasing slope of the frequency parameter Ω will be. At the same time, according to Figure 11, the rule of frequency parameter Ω of the same modal order under different boundary conditions can be obtained as follows: CCC > CCF > SSF > EEF. Since the spring stiffness value of the fixed support boundary (C) > the spring stiffness value of the simply supported boundary (S) > the spring stiffness value of the elastic boundary (E) > the spring stiffness value of the free boundary (F), it can be deduced that the natural frequency of the coupling system increases with the increase of the spring stiffness value.

The influence of the parameter conditions of composite-laminated curved beams on the vibration characteristics of composite-laminated rotationally stiffened plates also needs to be studied. Table 5 takes the stiffened annular sector and annular plate as examples and gives the frequency parameter Ω of the first eight orders for two kinds of composite-laminated rotationally stiffened plates with different numbers and sizes of stiffeners. The maximum number of stiffeners n is 3, where stiffener 1 is at $R_p/2$, stiffener 2 is at $R_p/3$, and stiffener 3 is at $2R_p/3$. The geometric parameters of the two kinds of composite-laminated rotationally stiffened plates in the calculation example are $R_1 = 1$ m, $R_2 = 2.2$ m, $R_{b1} = 1.6$ m, $R_{b2} = 1.4$ m, $R_{b3} = 1.8$ m, and $h_p = 0.035$ m. The plate structure is set as glass fiber resin, the stiffener material is set as graphite fiber resin, and the angle-ply is set as [−45°/0°/45°]. It can be seen from Table 5 that compared with the plate structure without stiffeners, when the number of stiffeners n is 1, the frequency parameter Ω of most orders of stiffened annular sector plates and stiffened annular plates tends to increase, and the degree of increase is related to the size parameter of stiffeners, while the frequency parameter Ω will decrease with the increase of the number of stiffeners n. It can be seen from Table 5 that compared with the plate structure without stiffeners, the frequency

Q235 steel
Test results

$f_3 = 406.76$ Hz
Calculation results of present method $f_5 = 767.72$ Hz $f_7 = 936.57$ Hz

$f_3 = 404.55$ Hz $f_5 = 754.46$ Hz $f_7 = 1007.36$ Hz
Carbon fiber composite material
Test results

$f_2 = 89.18$ Hz $f_7 = 520.35$ Hz $f_9 = 850.75$ Hz
Calculation results of present method

$f_2 = 86.09$ Hz $f_7 = 529.32$ Hz $f_9 = 878.56$ Hz
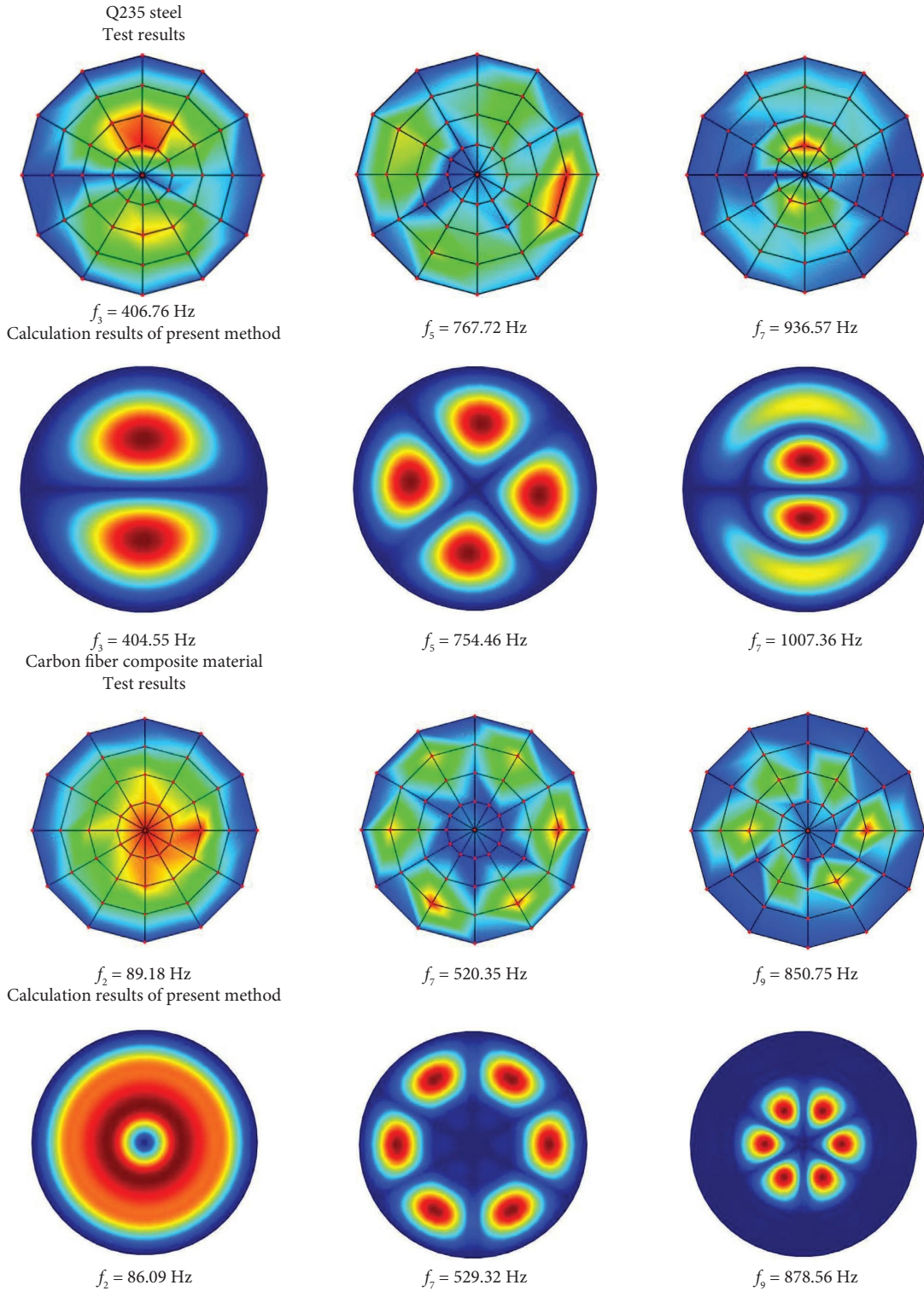
FIGURE 10: Natural frequencies and modal shapes of stiffened circular plate obtained by test and this method.

parameter Ω of most orders of stiffened annular sector plates and stiffened annular plates tends to increase when the number of stiffeners n is 1, and the degree of increase is related to the size parameter of stiffeners, while the frequency parameter Ω will decrease with the increase of the number of stiffeners n.

Figure 12 shows the modal shapes corresponding to the first two frequency parameters of the stiffened annular sector plate under different numbers of stiffeners, which more intuitively reflects the influence of stiffeners on the structure of the rotational plate. The size and material parameters of the stiffened annular sector plate are the same as those in

TABLE 4: Frequency parameter Ω of stiffened composite circular sector plate under different boundary and parameter conditions.

Boundary condition	Angle-ply	ϑ	Modal order							
			1	2	3	4	5	6	7	8
SSF	[0°/90°]	90°	5.797	8.852	13.234	17.199	18.315	19.821	21.831	22.419
		180°	5.363	6.351	7.923	9.725	9.888	12.097	12.612	14.491
		270°	5.092	5.781	6.572	6.915	7.630	8.873	9.255	10.250
	[90°/0°/90°]	90°	4.619	8.080	12.924	13.823	18.832	18.898	19.251	19.916
		180°	4.161	5.294	7.066	9.224	9.469	11.680	12.183	13.681
		270°	4.023	4.628	5.557	6.580	6.744	8.113	8.668	9.628
CCF	[0°/90°]	90°	8.207	11.190	15.607	18.583	20.855	22.816	23.771	26.580
		180°	7.634	8.732	10.026	10.209	12.106	12.698	14.291	16.709
		270°	6.260	8.199	8.282	8.935	9.300	9.919	11.098	12.436
	[90°/0°/90°]	90°	6.536	10.139	15.326	16.746	19.513	21.686	22.733	23.480
		180°	6.032	7.157	8.927	9.660	11.140	12.303	13.704	16.560
		270°	5.633	6.505	6.961	7.392	8.574	8.695	9.955	11.511
CCC	[0°/90°]	90°	9.601	13.684	18.862	23.991	24.864	30.352	31.681	37.238
		180°	8.234	9.531	11.272	13.558	15.804	18.717	21.293	22.849
		270°	7.912	8.573	9.471	10.608	11.907	12.856	13.393	14.946
	[90°/0°/90°]	90°	8.337	13.307	19.553	19.834	27.063	27.566	34.966	36.190
		180°	6.549	8.111	10.226	12.775	15.615	16.757	18.889	19.482
		270°	6.196	6.957	8.042	9.393	10.911	12.562	12.661	14.496
E^2E^2F	[0°/90°]	90°	1.041	3.963	4.724	5.332	6.067	7.035	7.982	9.027
		180°	0.785	3.826	4.030	4.472	5.062	5.310	5.813	6.732
		270°	0.669	3.788	3.855	4.088	4.385	4.757	5.200	5.300
	[90°/0°/90°]	90°	1.026	3.563	4.147	4.610	6.208	7.162	7.765	8.587
		180°	0.771	3.393	3.730	4.112	4.316	5.048	5.982	6.920
		270°	0.653	3.344	3.493	3.818	4.102	4.212	4.680	5.235

(a)

(b)
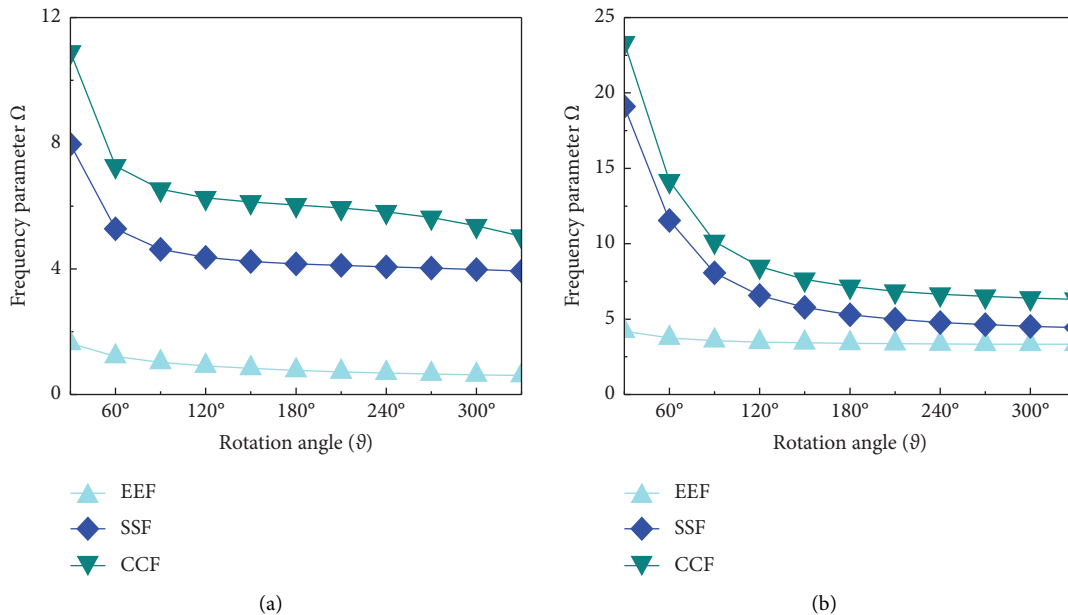
FIGURE 11: Continued.

(c)

(d)
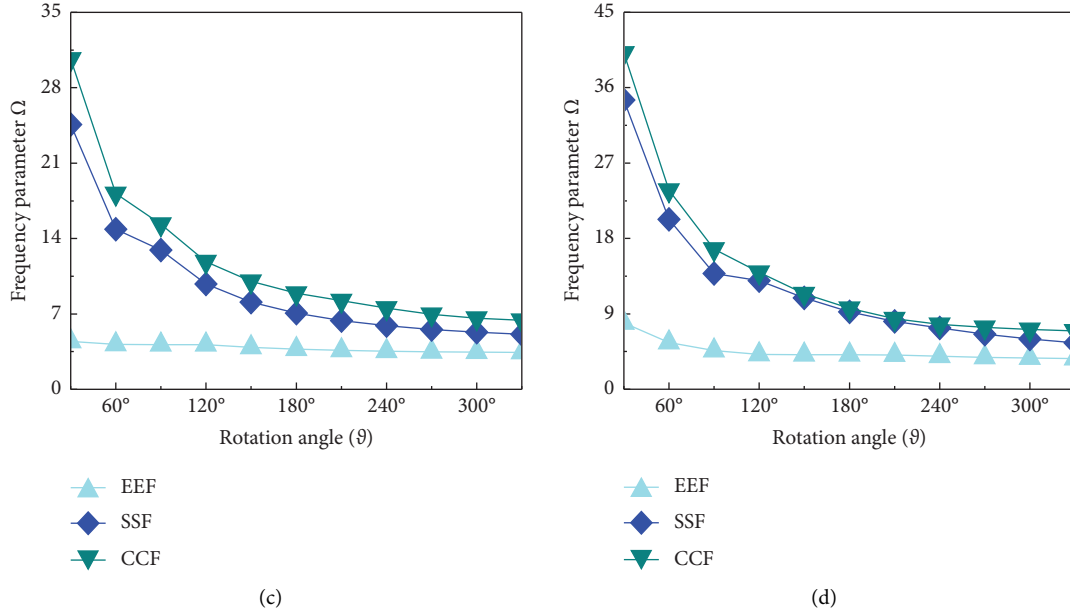
FIGURE 11: The change curve of frequency parameter Ω varies with rotation angle ϑ of stiffened composite circular sector plate under different boundary conditions. (a) First order. (b) Second order. (c) Third order. (d) Fourth order.

TABLE 5: Frequency parameter Ω of stiffened composite annular sector plate and stiffened composite annular plate with different numbers and sizes of stiffeners.

Number of stiffeners n	Modal order							
	1	2	3	4	5	6	7	8
$b_1 = b_2 = b_3 = 0.1$m, $h_1 = h_2 = h_3 = 0.08$m								
Stiffened annular sector plate; $\vartheta = 180°$, CCCC								
$n = 0$	5.124	5.129	5.240	5.569	6.217	7.245	8.601	10.287
$n = 1$	3.489	6.704	9.949	13.155	13.443	15.967	16.248	18.928
$n = 2$	3.618	6.943	7.080	9.327	10.269	10.968	12.201	13.530
$n = 3$	3.541	5.758	6.706	8.076	8.263	9.706	9.845	9.997
Stiffened annular plate: $\vartheta = 360°$, CC								
$n = 0$	5.101	5.101	5.124	5.124	5.135	5.138	5.138	5.339
$n = 1$	1.094	3.467	3.467	6.659	6.659	9.880	9.880	12.432
$n = 2$	1.118	3.603	3.603	6.155	6.913	6.913	7.073	7.073
$n = 3$	1.201	3.528	3.528	4.644	5.749	5.749	6.680	6.680
$b_1 = b_2 = b_3 = 0.05$m, $h_1 = h_2 = h_3 = 0.04$m								
Stiffened annular sector plate: $\vartheta = 180°$, CCCC								
$n = 0$	5.124	5.129	5.240	5.569	6.217	7.245	8.601	10.287
$n = 1$	2.806	4.961	7.239	9.548	11.857	14.154	16.403	18.061
$n = 2$	2.898	5.166	7.543	8.189	9.262	9.941	10.820	12.318
$n = 3$	2.900	5.067	6.209	7.343	7.519	9.317	9.629	10.076
Stiffened annular plate: $\vartheta = 360°$, CC								
$n = 0$	5.101	5.101	5.124	5.124	5.135	5.138	5.138	5.339
$n = 1$	1.513	2.778	2.778	4.895	4.895	7.137	7.137	9.405
$n = 2$	1.511	2.871	2.871	5.104	5.104	7.451	7.451	7.800
$n = 3$	1.616	2.876	2.876	5.011	5.011	5.709	6.197	6.197

Table 5; the width and thickness of the stiffener are $b_1 = b_2 = b_3 = 0.1$ m, $h_1 = h_2 = h_3 = 0.08$ m. It can be seen from Figure 12 that the vibration modal diagram at the location of the stiffener is significantly curved, which indicates that the laminated plate and laminated curved beam structure in the model of composite laminated rotationally stiffened plate are coupled.

Taking the stiffened composite circular plate as an example, the variation curve of the frequency parameter Ω with the thickness h_n of the laminated curved beam under the same thickness-to-width ratio is shown in Figure 13. The number of stiffeners n is 2, stiffener 1 is at $R_p/3$, and stiffener 2 is at $2R_p/3$. The constant geometric parameters of stiffened circular plate in the calculation example are:\ $R_1 = 0$ m,

Stiffened annular sector plate:
First order

$n = 0$ $n = 1$ $n = 2$ $n = 3$

Second order

$n = 0$ $n = 1$ $n = 2$ $n = 3$
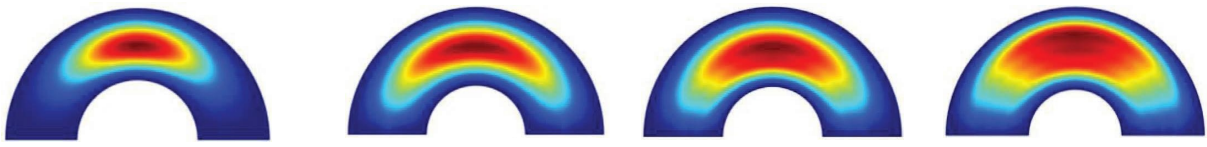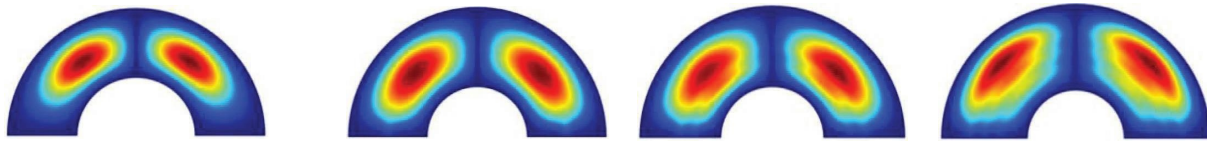
FIGURE 12: The first two order modal shapes of stiffened annular sector plate with different numbers of stiffeners.
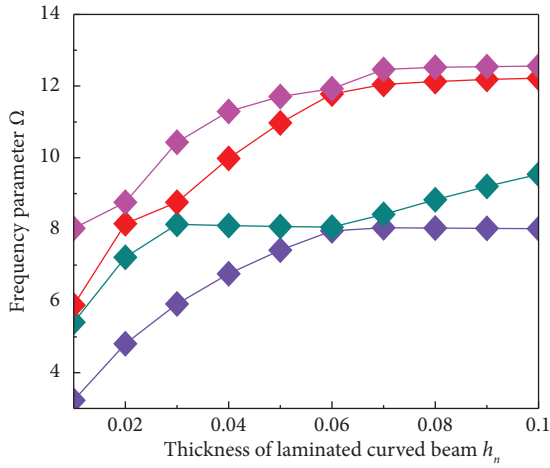
(a)
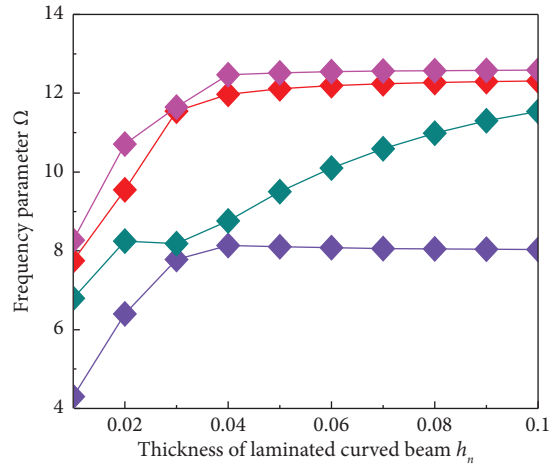
(b)

FIGURE 13: Continued.

(c)

(d)
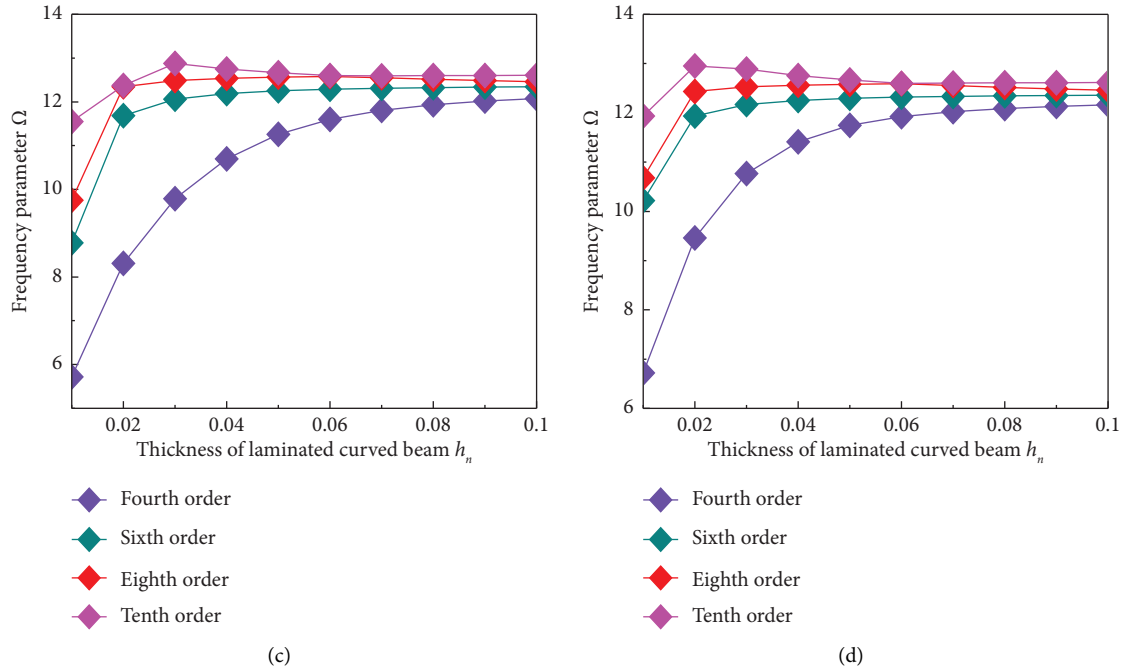
FIGURE 13: Variation curve of frequency parameter Ω with the thickness of laminated curved beam for composite stiffened circular plate under the same thickness to width ratio. (a) $b_n/h_n = 0.5$, (b) $b_n/h_n = 1$, (c) $b_n/h_n = 2$, and (d) $b_n/h_n = 3$.
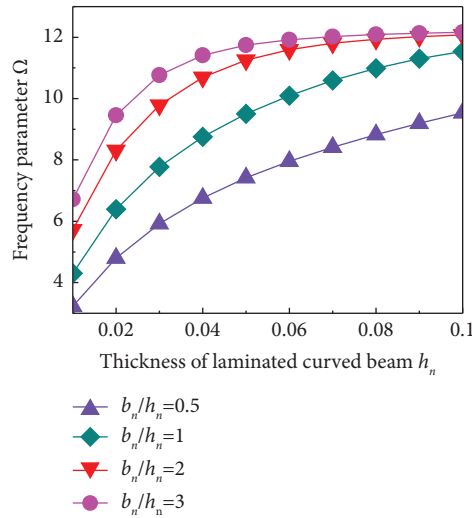
FIGURE 14: Variation curve of frequency parameter Ω with the thickness of laminated curved beam for composite stiffened circular plate under the different thickness to width ratio.

$R_2 = 1.8$ m, $R_{b1} = 0.6$ m, $R_{b2} = 1.2$ m, $h_p = 0.02$ m, $b_1 = b_2$, and $h_1 = h_2$. The boundary condition is S, the plate structure and stiffener material are set as glass fiber resin, and the angle-ply is set as [0°/60°]. According to the analysis in Figure 13, the frequency parameter Ω of the same order increases with the increase of the thickness of the laminated curved beam h_n under the same thickness-to-width ratio. The variation curve of the frequency parameter Ω with the thickness h_n of the laminated curved beam under the different thickness-to-width ratio is shown in Figure 14. The geometric and material parameters in Figure 14 are the same as those in

Figure 13, The mode is the fourth order. It can be seen from Figure 14, the frequency parameter Ω increases with the increase of the thickness-to-width ratio; it means that as the width of the laminated curved beam increases, the frequency parameter Ω increases. To sum up, the thickness and width of the laminated curved beam are positively correlated with the frequency parameter Ω of the composite-laminated rotationally stiffened plate.

Continuing with the discussion on the effect of material parameters of the stiffeners on the natural frequencies of composite-laminated rotationally stiffened plates, the effect of
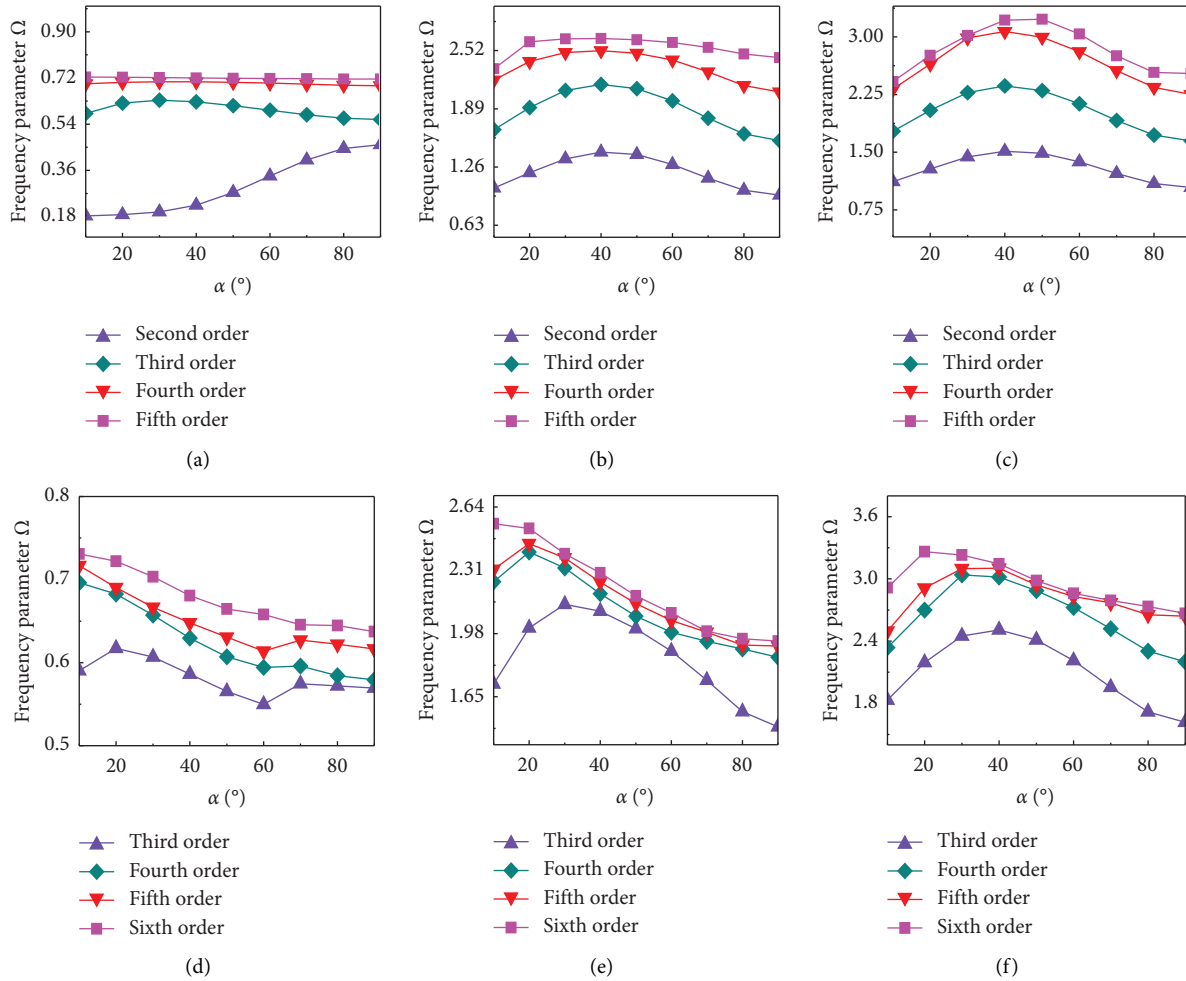
FIGURE 15: Variation curve of frequency parameter Ω with the layer angle of the stiffeners under different boundary conditions. (a) $[0/\alpha°/0]$ EEEF. (b) $[0/\alpha°/0]$ SSSF. (c) $[0/\alpha°/0]$ CCCF. (d) $[0/\alpha°/0/\alpha°]$ EEEF. (e) $[0/\alpha°/0/\alpha°]$ SSSF. (f) $[0/\alpha°/0/\alpha°]$ CCCF.

the layer angle of the stiffeners on the frequencies is investigated. Figure 15 illustrates the effect of varying layer angle of the stiffeners under different boundary conditions and two different layer schemes on the natural frequencies of composite-laminated rotationally stiffened plates. In this particular case, the geometric parameters of the composite-laminated rotationally stiffened plate are as follows: $R_0 = 1$ m, $R_1 = 2$ m, $b_1 = 0.06$ m, and $h_1 = 0.04$ m, with a rotation angle of 90°. The materials of the laminated plate and the laminated beam (stiffener) are glass epoxy resin with the following material parameters: $E_1 = 185$ GPa, $E_2 = 10.9$ GPa, $G_1 = G_2 = G_3 = 7.3$ GPa, $\mu = 0.28$, and $\rho_p = 1600$ kg/m^3. The number of laminated beams is 1, located at $R_p/2$. From Figure 15, it can be observed that under both layer schemes, for the SSSF and CCCF boundary conditions, the variation in the layer angle of the stiffener exhibits a similar trend in affecting the natural frequencies of the composite laminated rotationally stiffened plates. Within the range of 0–90°, the natural frequencies generally increase with an increase in the layer angle before decreasing. However, for the EEEF boundary condition, under the $[0/\alpha°/0]$ layer scheme, except for the second order, the other natural frequencies remain relatively constant within the

0–90° range. Under the $[0/\alpha°/0/\alpha°]$ layer scheme, except for the second order, the overall trend of the other natural frequencies within the 0–90° range is a decrease with an increase in the layer angle. This discrepancy is mainly due to the different influences of the boundary conditions on the stiffness of the structure.

Next, the effect of the anisotropy of the stiffener on the frequencies of composite-laminated rotationally stiffened plate is investigated. Figure 16 illustrates the effect of varying anisotropy of the stiffener on the natural frequencies of composite-laminated rotationally stiffened plates under different boundary conditions. The anisotropy of the composite material is defined as E_1/E_2. In this example, the geometric parameters of the composite-laminated rotationally stiffened plate are $R_0 = 1$ m, $R_1 = 3$ m, $b_1 = 0.06$ m, and $h_1 = 0.04$ m, with a rotation angle of 180°. The material for both the laminated plate and the laminated beam (stiffener) is glass epoxy resin, with material parameters remaining unchanged except for E_1, which varies as a parameter, consistent with Figure 15. The number of laminated beams is 1, located at $R_p/4$, and the layer scheme of the stiffener is $[0/90°/0/90°]$. From Figure 16, it can be observed
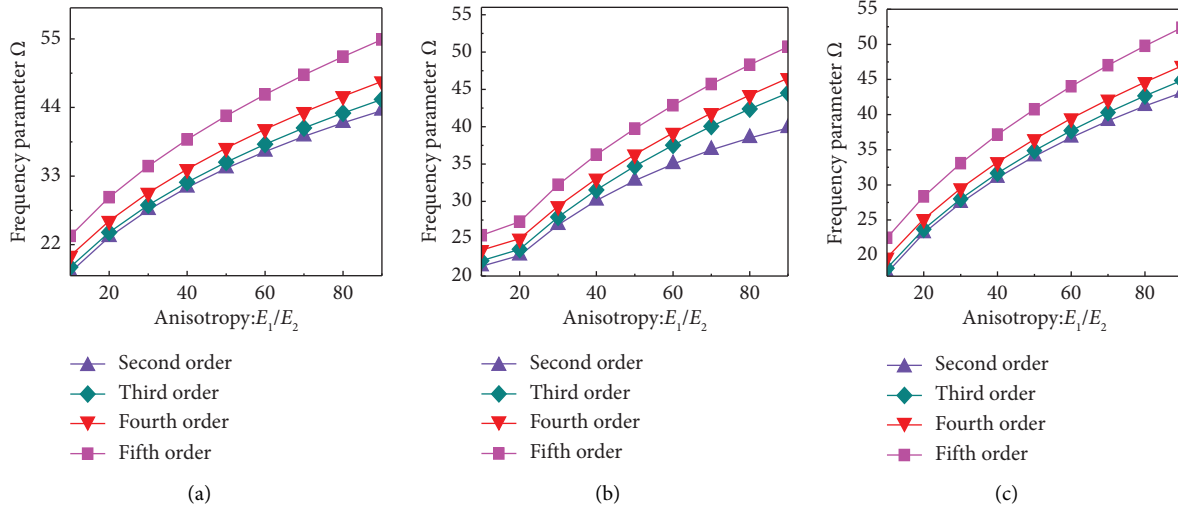
FIGURE 16: Variation curve of frequency parameter Ω with the anisotropy of the stiffener under different boundary conditions. (a) EFEF. (b) SFSF. (c) CFCF.

TABLE 6: The first eight-order frequency parameter Ω of rotationally isotropic stiffened plates under different boundary conditions.

Boundary condition	Method	Modal order							
		1	2	3	4	5	6	7	8
		Stiffened annular sector plate: $R_1 = 0.4$m, $R_{b1} = 1$m, $\vartheta = 120°$							
CFCF	Present method	0.802	1.373	2.750	4.299	4.935	5.893	7.603	10.383
	FEM	0.759	1.421	2.961	4.194	5.067	6.118	7.614	10.098
CCCC	Present method	5.772	9.749	14.273	14.829	17.379	19.576	23.227	24.210
	FEM	5.659	9.996	13.391	15.117	17.383	19.761	23.439	25.070
		Stiffened circular sector plate: $R_1 = 0$m, $R_{b1} = 0.8$m, $\vartheta = 120°$							
CFC	Present method	2.532	5.613	7.666	9.431	11.538	12.499	14.468	16.949
	FEM	2.720	5.396	7.747	9.472	11.828	13.129	14.106	17.020
CCC	Present method	5.456	9.206	11.850	12.558	16.391	17.845	18.342	20.828
	FEM	5.343	9.129	11.096	12.711	16.457	17.843	18.249	21.000
		Stiffened annular plate: $R_1 = 0.4$m, $R_{b1} = 1$m, $\vartheta = 360°$							
CF	Present method	0.735	0.735	0.915	0.926	0.926	1.747	1.748	3.194
	FEM	0.744	0.744	0.906	0.931	0.931	1.883	1.883	3.078
CC	Present method	4.280	4.655	4.655	5.404	5.404	7.572	7.583	10.479
	FEM	4.397	4.618	4.619	5.589	5.589	7.688	7.689	10.744
		Stiffened circular plate: $R_1 = 0$m, $R_{b1} = 0.8$m, $\vartheta = 360°$							
F	Present method	0.802	0.802	1.307	1.599	1.605	2.635	2.635	2.762
	FEM	0.780	0.780	1.443	1.678	1.679	2.633	2.633	2.756
C	Present method	1.404	2.514	2.515	4.387	4.387	4.780	7.008	7.018
	FEM	1.430	2.661	2.661	4.644	4.645	4.857	7.252	7.253

that under different boundary conditions, within the range of 0–100, the natural frequencies of the composite-laminated rotationally stiffened plate increase with an increase in the anisotropy of the stiffener material.

The stiffened plate model established in this paper can not only analyze the stiffened composite plate structure but also study the vibration characteristics of isotropic stiffened plate structure by changing the material parameter settings. Table 6 shows the first 8-order frequency parameter Ω of the rotationally isotropic stiffened plate under different boundary conditions and compares it with the results of the finite element method. The number of stiffeners n is 1, and

the stiffener is located at $R_p/2$. The invariant geometric parameters of the rotationally stiffened plate in the calculation example are $R_2 = 1.6$ m, $h_p = 0.03$ m, $b_1 = 0.06$ m, and $h_1 = 0.04$ m. The plate structure and stiffener material are set as isotropic material steel. As shown in Table 6, the results obtained by this method and the finite element method are relatively close, and the error is less than 5%.

In the process of free vibration analysis, it can be found that compared with the finite element method, the present method does not need to establish a new model when calculating examples with different material and size parameters but only needs to change the relevant parameters in

the program, which saves more time. At the same time, the present method can directly parameterize the influencing factors and analyze the influencing mechanism of the relevant parameters by changing the relevant schemes.

4. Conclusions

Based on the improved Fourier series method and the Rayleigh–Ritz method, a unified analytical model for the vibration characteristics of composite-laminated rotationally stiffened plates is established in this paper. First, the admissible displacement function of laminated plates and laminated curved beams are established by two-dimensional and one-dimensional improved Fourier series methods; second, the energy function of laminated plate and laminated curved beam in stiffened plate is established, and the potential energy coupling between laminated plate and laminated curved beam is introduced to obtain the total energy function of composite-laminated rotationally stiffened plate structure; finally, the total energy function equation is solved according to the Rayleigh–Ritz method. The free vibration and structural model test of composite-laminated rotationally stiffened plates are studied, and the following important conclusions are obtained:

(1) When the cutoff value of admissible displacement function of laminated plate and laminated curved beam is $M_p \times N_p = 18 \times 18$, $M_b = 50$, the natural frequencies of the unified analysis model for the vibration characteristics of composite-laminated rotationally stiffened plate structure constructed by this method basically converge, and the error between the natural frequencies of each order and the finite element simulation is 6.38%, and the spring stiffness value also converge at 10^{10}.

(2) The error between the test results and the calculation results of this method in the model correctness verification is 7.56%, and the modal shapes obtained by the two methods are very close, which verifies the correctness of the unified analysis model of composite-laminated rotationally stiffened plate structure established in this section.

(3) Under the condition of free vibration, the natural frequency of composite-laminated rotationally stiffened plates decreases with the increase of rotation angle, increases with the increase of boundary spring stiffness, decreases with the increase of the number of stiffeners, and increases with the increase of the thickness and width of laminated curved beams.

Data Availability

The data used to support the findings of this study are available from the corresponding author upon request.

Conflicts of Interest

The authors declare that they have no conflicts of interest.

References

[1] T. Irie, G. Yamada, and S. Aomura, "Free vibration of radially stiffened annular plate," *Bulletin of JSME*, vol. 23, no. 175, pp. 76–82, 1980.

[2] A. A. Jafari and M. Bagheri, "Free vibration of rotating ring stiffened cylindrical shells with non-uniform stiffener distribution," *Journal of Sound and Vibration*, vol. 296, no. 1-2, pp. 353–367, 2006.

[3] X. Qin, Y. Shen, W. Chen, J. Yang, and L. Peng, "Bending and free vibration analyses of circular stiffened plates using the FSDT mesh-free method," *International Journal of Mechanical Sciences*, vol. 202, 2021.

[4] M. E. Golmakani and M. Mehrabian, "Nonlinear bending analysis of ring-stiffened circular and annular general angle-ply laminated plates with various boundary conditions," *Mechanics Research Communications*, vol. 59, pp. 42–50, 2014.

[5] M. E. Golmakani and M. Kadkhodayan, "Large deflection thermoelastic analysis of functionally graded stiffened annular sector plates," *International Journal of Mechanical Sciences*, vol. 69, pp. 94–106, 2013.

[6] X. Ou, X. Yao, R. Zhang, X. Zhang, and Q. Han, "Nonlinear dynamic response analysis of cylindrical composite stiffened laminates based on the weak form quadrature element method," *Composite Structures*, vol. 203, pp. 446–457, 2018.

[7] L. X. Peng, J. Xiang, X. Qin, Z. Xie, and S. Chen, "A meshless method for geometric nonlinear analysis of arbitrary polygonal and circular stiffened plates," *International Journal of Non-linear Mechanics*, vol. 148, 2023.

[8] A. Bhimaraddi, P. J. Moss, and A. J. Carr, "Finite element analysis of orthogonally stiffened annular sector plates," *Journal of Engineering Mechanics*, vol. 115, no. 9, pp. 2074–2088, 1989.

[9] N. K. Gupta and N. Gupta, "Response of thin walled transversely stiffened clamped circular plates under uniform impulsive loads," *Thin-Walled Structures*, vol. 182, 2023.

[10] C. Itu, A. Öchsner, S. Vlase, and M. I. Marin, "Improved rigidity of composite circular plates through radial ribs," *Proceedings of the Institution of Mechanical Engineers, Part L: Journal of Materials: Design and Applications*, vol. 233, no. 8, pp. 1585–1593, 2018.

[11] G. J. Turvey and M. Salehi, "Elasto-plastic large deflection response of pressure loaded circular plates stiffened by a single diametral stiffener," *Thin-Walled Structures*, vol. 46, no. 7-9, pp. 991–1002, 2008.

[12] H. Zhang, D. Shi, S. Zha, and Q. Wang, "Vibro-acoustic analysis of the thin laminated rectangular plate-cavity coupling system," *Composite Structures*, vol. 189, pp. 570–585, 2018.

[13] D. Shi, S. Zha, H. Zhang, and Q. Wang, "Free vibration analysis of the unified functionally graded shallow shell with general boundary conditions," *Shock and Vibration*, vol. 2017, Article ID 7025190, 19 pages, 2017.

[14] D. Shi, H. Zhang, Q. Wang, and S. Zha, "Free and forced vibration of the moderately thick laminated composite rectangular plate on various elastic winkler and pasternak

foundations," *Shock and Vibration*, vol. 2017, Article ID 7820130, 23 pages, 2017.

[15] Y. Zhou, Q. Wang, D. Shi, Q. Liang, and Z. Zhang, "Exact solutions for the free in-plane vibrations of rectangular plates with arbitrary boundary conditions," *International Journal of Mechanical Sciences*, vol. 130, pp. 1–10, 2017.

[16] Q. Wang, X. Cui, B. Qin, Q. Liang, and J. Tang, "A semi-analytical method for vibration analysis of functionally graded (FG) sandwich doubly-curved panels and shells of revolution," *International Journal of Mechanical Sciences*, vol. 134, pp. 479–499, 2017.

[17] Q. Wang, X. Cui, B. Qin, and Q. Liang, "Vibration analysis of the functionally graded carbon nanotube reinforced composite shallow shells with arbitrary boundary conditions," *Composite Structures*, vol. 182, pp. 364–379, 2017.

[18] W. L. Li, "Free vibrations of beams with general boundary conditions," *Journal of Sound and Vibration*, vol. 237, no. 4, pp. 709–725, 2000.

[19] W. L. Li, "Comparison of Fourier sine and cosine series expansions for beams with arbitrary boundary conditions," *Journal of Sound and Vibration*, vol. 255, no. 1, pp. 185–194, 2002.

[20] M. S. Qatu, *Vibration of Laminated Shells and Plates*, Elsevier, Amsterdam, The Netherlands, 2004.

[21] H. Zhang, Y. Ding, L. He, C. Shuai, and C. Jiang, "The vibro-acoustic characteristics analysis of the coupled system between composite laminated rotationally stiffened plate and acoustic cavities," *Applied Sciences*, vol. 14, no. 3, p. 1002, 2024.